Optimal Binary Power Control and Passive Beamforming for RIS-Assisted Spectrum Sharing

Priyanka Das, *Senior Member, IEEE*, Sumukha Kashyap, *Student Member, IEEE*, Rimalapudi Sarvendranath, *Senior Member, IEEE*, and Amrita Mishra, *Member, IEEE*

***Abstract*—Reconfigurable intelligent surface (RIS)-assisted underlay spectrum sharing system improves the utilization of the wireless spectrum in an energy-efficient manner. For it, joint power control and RIS phase shift optimization is studied under an instantaneous interference constraint. We focus on a less-explored yet practical average interference-constrained secondary system, in which a secondary source (S) employs binary power control. We systematically develop an optimal rule to minimize an average symbol error probability (SEP) at a secondary destination (D) under an average interference constraint. It jointly optimizes binary transmit power of S and RIS phase shifts. We further propose two low-complexity rules–1) maximum signal power (MSP) rule and 2) low interference (LI) rule. The MSP rule maximizes the received signal power at D. The LI rule reduces the received interference power at the primary receiver. We analyze the average interference power caused by the low-complexity rules and derive insightful asymptotic expressions in closed-form considering spatial correlation. Numerical results demonstrate the impact of discrete phase shifts, imperfect channel state information (CSI), and RIS mutual coupling effect on the average SEP and the average interference power. We show that the optimal rule minimizes the average SEP, the LI rule is near-optimal when the interference constraint is strict, and in the interference-unconstrained regime, the MSP rule outperforms the LI rule. We further study performance–complexity tradeoff of instantaneous CSI-based versus codebook-based design for RIS phase shift control in underlay spectrum sharing system.**

***Index Terms*—Reconfigurable intelligent surface, spectrum sharing, binary power control, symbol error probability, average interference constraint.**

I. Introduction

RECONFIGURABLE intelligent surface (RIS)-assisted spectrum sharing enables efficient utilization of the limited wireless spectrum in an energy-efficient manner. It is considered as an effective solution to increase both spectral efficiency and energy efficiency [2]. They become two essential criteria for designing future wireless networks, since not enough spectrum is available to support the upcoming sixth-generation (6G) applications such as augmented reality (AR), virtual reality (VR), immersive communication, and hyper reliable and low latency communication [3], and especially, for designing energy-constrained systems such as Internet of Things (IoT) networks. Recognizing the need for more spectrum, the world radiocommunication conference (WRC) 2023 identified the bands 4.4-4.8 GHz, 7.125-8.4 GHz, and 14.8-15.35 GHz for the potential use by 6G applications and initiated sharing and compatibility studies to develop regulations that protect the incumbent services [4]. The spectrum regulators around the world have also accepted the need for the spectrum sharing. The Federal Communications Commission (FCC) in the USA is allowing for shared spectrum usage in the 3.5 GHz and the 6 GHz bands [5]. Several wireless standards, such as citizens broadband radio service (CBRS), MulteFire, 5G NR-Unlicensed, and IEEE 802.11be, focus on spectrum sharing [6], [7]. Furthermore, 6G is being designed from the beginning to share spectrum with other radio access technologies such 5G-NR [8].

Different from a listen-before-talk approach, in which a low-priority secondary user (SU) transmits only when a high priority primary user (PU) is off, as typically considered in most of the current spectrum sharing standards, we focus on an underlay mode of spectrum sharing. In it, the SU transmits simultaneously on the same frequency band as the PU while ensuring that the interference caused to the primary receiver is constrained [9], [10]. This interference constraint protects the primary from the excessive interference from the SU. However, it limits the performance of the secondary system.

Meanwhile, RIS is envisioned to be a promising 6G technology to cost-effectively improve the performance of the secondary system without requiring power-consuming circuits while adhering to the primary interference constraints [11], [12]. It is made up of a large number of reconfigurable passive reflective elements. Each reflective element of the RIS can be programmed to induce a given phase shift such that the reflected signal forms a beam in the desired direction. This is referred to as passive beamforming due to the absence of active radio frequency (RF) chains. To enable this passive beamforming with low training overhead, several codebook-based schemes have been studied [13], [14], [15]. It is shown that an environment-aware codebook design that exploits statistical channel state information (CSI) performs better with lower

Received 7 December 2025; revised 10 May 2026; accepted 24 July 2026. Date of publication 7 August 2026; date of current version 20 August 2026. This work was supported by IIITB COMET Foundation, established under the Advanced Communication Systems vertical of the National Mission on Interdisciplinary Cyber-Physical Systems (NM-ICPS), Department of Science and Technology, Govt. of India. The work of Rimalapudi Sarvendranath was supported by the DST INSPIRE Research Grant and SERB Research under Grant SRG/2023/000070. An earlier version of this paper was presented in part at the IEEE Global Communications Conference (Globecom) Workshop, in December 2023 [DOI: 10.1109/TCOMM.2026.3721640]. The associate editor coordinating the review of this article and approving it for publication was C. Liaskos. *(Corresponding author: Priyanka Das.)*

Priyanka Das and Amrita Mishra are with the Department of Electronics and Communication Engineering, International Institute of Information Technology Bangalore (IIIT-B), Bengaluru 560100, India (e-mail: priyanka.das@iiitb.ac.in; amrita.mishra@iiitb.ac.in).

Sumukha Kashyap is with the Department of Electrical Engineering, IIT Madras, Chennai 600036, India (e-mail: ee24d038@smail.iitm.ac.in).

Rimalapudi Sarvendranath is with the Department of Electrical Engineering, IIT Tirupati, Andhra Pradesh 517619, India (e-mail: sarvendranath@iittp.ac.in).

Digital Object Identifier 10.1109/TCOMM.2026.3721640

0090-6778 © 2026 IEEE. All rights reserved, including rights for text and data mining, and training of artificial intelligence and similar technologies. Personal use is permitted, but republication/redistribution requires IEEE permission.
See https://www.ieee.org/publications/rights/index.html for more information.

Authorized licensed use limited to: Indian Institute of Technology. Downloaded on November 03,2026 at 17:26:23 UTC from IEEE Xplore. Restrictions apply.

TABLE I
COMPARATIVE STUDY OF RELATED WORKS FOR RIS-ASSISTED SPECTRUM SHARING SYSTEM

Paper	Power control	Fading model	Simulation/Analysis	Constraint	Objective	CSI
[11]	Continuous	Independent Rayleigh	Simulation	PU SINR	Maximize rate	Perfect
[12]	Continuous	Independent Rayleigh	Simulation	Peak interference	Maximize rate	Perfect
[16]	Continuous	Independent Rayleigh	Simulation	Peak interference	Maximize rate	Perfect
[17]	Continuous	Independent Rayleigh	Simulation	Peak interference	Maximize rate	Perfect
[18]	Continuous	Independent Rayleigh	Simulation	Peak interference	Maximize rate	Perfect
[19]	Continuous	Independent Rayleigh	Simulation	Peak interference	Minimize power	Perfect
[20]	Continuous	Independent Rayleigh	Simulation	Peak interference	Minimize power	Imperfect
[21]	Continuous	Independent Rician	Simulation	Peak interference	Maximize rate	Perfect
[22]	Continuous	Independent Rician	Analysis (No direct link)	Peak interference	Maximize rate	Perfect
[2]	Continuous	Correlated Rician	Simulation	Peak interference	Maximize rate	Imperfect
[23]	Binary	Independent Rician	Analysis (Direct link)	Interference-Outage	Minimize SEP	Perfect
Proposed	Binary	*Correlated* Rician	Analysis (Direct link)	Average interference	Minimize SEP	Perfect (Analysis), Imperfect (Simulation)

complexity [13]. In [14], a dynamic codebook framework based on probabilistic learning is proposed. It is shown to have robust performance with limited training overhead. In [15], a pricing-based codebook approach that models RIS as a network resource is proposed, relying on precomputed RIS configurations. Unlike the conventional RIS system, for an RIS-assisted spectrum sharing system, the configured phase shifts of the RIS should improve the signal strength received at the secondary receiver while ensuring that the interference constraint at the primary receiver is met [1], [2], [11].

A. RIS-Assisted Spectrum Sharing [11], [12], [16], [17], [18], [19], [20], [21], [22], [24]

To control the interference caused to the primary receiver (X), two types of power control schemes, namely, *continuous power control* [2], [25], in which the secondary source (S) can transmit with any power value below a peak transmit power $P_{\max}$, and *binary power control* [1], [9], in which S transmits either with fixed transmit power $P_{\max}$ (on) or zero power (off) are considered in literature, as we discuss below.

i) Continuous Power Control Under Peak Interference Constraint: An alternating optimization (AO) algorithm is proposed in [12] to optimize the active beamforming at S and passive beamforming at the RIS to maximize the secondary system's sum rate under a peak interference constraint. A similar problem is studied in [2] under both perfect and imperfect CSI cases. A block coordinate descent (BCD) algorithm is proposed in [16] for a peak interference-constrained secondary system to optimize the precoding matrix at S and the passive beamforming vector at the RIS to maximize the weighted sum rate. In [17], through simulations, it is shown that a penalty dual decomposition based gradient projection algorithm improves the achievable rate of a peak interference-constrained secondary system.

A successive convex approximation (SCA)-based AO algorithm is proposed in [18] to improve the minimum rate of the users in an RIS assisted non-orthogonal multiple access-based spectrum sharing system. The performance of an AO algorithm that jointly optimizes the uplink and downlink phase shifts of the RIS elements with optimal time slots for wireless energy transfer on the downlink and wireless information transfer on the uplink is studied through simulations in [21]. Considering an independent channel gain model in [22], analytical expressions for the outage probability, ergodic capacity, and average bit error rate are derived for a peak interference-constrained secondary system when the direct link is blocked. A difference-of-convex algorithm that optimizes both active and passive beamforming is proposed in [19] to solve a non-convex quadratic problem that aims to minimize the transmit power at S subject to a peak interference constraint. Similarly, in [20], a successive convex approximation-based algorithm is proposed to minimize the transmit power at S.

ii) Continuous Power Control Under Primary Signal-to-Interference-plus-Noise Ratio (SINR) Constraint: With perfect CSI, an AO algorithm that optimizes the transmit power at S and the passive beamforming at the RIS to maximize the achievable rate of a secondary system that is subject to an instantaneous SINR constraint at the primary receiver is proposed in [11]. It has been extended to consider imperfect CSI and discrete phase shifts in [24].

iii) Binary Power Control [23]: For an interference-outage constrained secondary system, joint binary power control and RIS phase shift optimization problem is investigated in [23], aiming to minimize an average symbol error probability (SEP).

Table I presents the detailed literature survey highlighting the novel aspects of our model and analysis.

B. Novelty, Focus, and Contributions

We focus on minimizing the average SEP of an RIS-assisted spectrum sharing system. In it, a secondary source S employs *binary power control* (BPC) to communicate to a secondary destination (D) with the help of an RIS. We focus on satisfying the *average interference constraint* at the primary receiver X, which limits the fading-averaged interference power to be below a threshold.

We now list the novel aspects of the power control, interference constraint, channel model, objective considered, and analysis performed in the following:

i) Power Control: We employ BPC, which is different from the widely considered continuous power control for RIS-aided system [11], [12], [16], [17], [18], [19], [20], [21], [22]. As shown in [9] and [26], different techniques are required for the optimal binary transmit power. Moreover,

Authorized licensed use limited to: Indian Institute of Technology. Downloaded on November 03,2026 at 17:26:23 UTC from IEEE Xplore. Restrictions apply.

BPC enables the design of an efficient power amplifier and RF chain.

ii) Interference Constraint: Different from the widely studied instantaneous interference constraint [11], [12], [16], [17], [18], [19], [20], [21], [22], which requires perfect CSI, we consider a practical average interference constraint, which can handle noisy channel estimates [10], [27], [28].

iii) Channel Model: We consider a *correlated Rician* fading model for the RIS-aided channels, which is more generalized and different from the independent channel model considered in [11], [12], [16], [17], [18], [19], [20], [21], and [22] and Rayleigh fading model in [11], [12], [16], [17], [18], [19], and [20]. In practice, the channel gains to/from the RIS elements, which are arranged in a two-dimensional geometry, are shown to be correlated [29]. We further show the impact of RIS mutual coupling effect.

iv) Analysis: We derive analytical expressions for the correlated channel model considering direct link, unlike [11], [12], [16], [17], [18], [19], [20], and [21], which study the performance of an RIS-assisted spectrum sharing systems through simulations. Furthermore, our analysis for the correlated Rician fading model is involved compared to the analysis done for a simpler independent channel model without a direct link in [22].

v) Objective: We minimize the average SEP, which is different from the widely studied problem of rate maximization [11], [12], [16], [17], [18], [21], [22] and transmit power minimization [19], [20]. The SEP is a classical measure of the reliability of communication [25], [30], which requires a different power control and RIS phase shift design scheme [9], [26].

Our specific contributions are as follows:

1) *Optimal Rule:* We systematically develop an optimal rule for joint BPC at S and passive beamforming at the RIS to minimize the average SEP at D subject to an average interference constraint. It chooses binary transmit power ($P_{\max}$ or 0) at S and RIS phase shifts that minimizes a linear combination of the instantaneous SEP at D and the instantaneous interference power at X scaled by an interference penalty factor δ, which is chosen to satisfy the average interference constraint with equality.
2) *Low-Complexity Rules:* We also propose two low-complexity rules for BPC and RIS passive beamforming: (i) *Low Interference (LI) rule:* It configures the RIS phases such that the interference signal through the direct link from S to X is out of phase with the interference signal received at X through RIS and (ii) *Maximum Signal Power (MSP) rule:* It configures the RIS phases such that the received signal through direct link from S to D is in phase with the received signal at D through RIS. Both the rules transmit with the maximum power $P_{\max}$ if the equivalent interference channel power gain from S to X is below a threshold and with zero power otherwise. We further analyze the computational complexity of all three proposed schemes.
3) *Analysis:* We derive closed-form expressions for the average interference power at X when the RIS phases are adjusted according to the MSP and LI rules, considering the RIS channel correlation. These results help in characterizing the optimal, LI, and MSP rules better. We also analyze the asymptotic average interference power for large number of RIS reflective elements (M).
4) *Numerical Results:* Our numerical results verify the performance analyses and characterize the effect of various system parameters such as location of various nodes, M, interference threshold, peak transmit power, channel correlation, and discrete phase shifts on the average SEP. Benchmarking results shows that the optimal rule minimizes the average SEP. The LI rule is near-optimal and outperforms the MSP rule in the interference-constrained regime. The MSP and the optimal rules provide similar performance in the interference-unconstrained regime.
5) *Impact of RIS Mutual Coupling, Imperfect CSI, and Codebook-based RIS Phase Control:* To capture the mutual coupling effect of the RIS reflecting elements, we further show the performance of the proposed schemes under an alternate scattering matrix-based correlation model. Moreover, we study the impact of imperfect CSI on the average SEP and average interference power. We further compare the proposed instantaneous CSI-based RIS phase control to a codebook-based RIS phase control scheme and bring out performance versus complexity trade-offs.

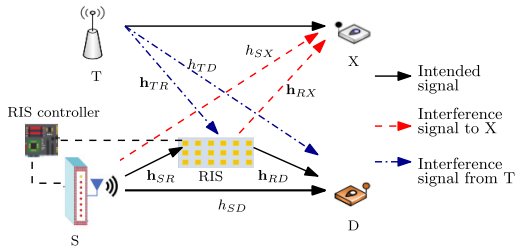


Fig. 1. An underlay spectrum sharing system with RIS.

Our paper extends the conference version [1]: i) Two low-complexity rules have been added in addition to the optimal rule. ii) RIS channel model has been extended to consider the spatial correlation, unlike the independent channel model in [1]. iii) The analytical expressions are derived considering spatial correlation, which is a non-trivial extension. iv) Valuable insights have been provided using asymptotic expressions derived. v) Performance benchmarking and numerical results have been extended to include channel correlation, discrete phase shifts, and the impact of more system parameters.

II. System Model

Fig. 1 illustrates our system model of an RIS-assisted underlay spectrum sharing system. In the secondary system, a secondary source S transmits data to a secondary destination D with the help of an RIS R having M reflective elements with minimum inter-element spacing d_v m. The primary system consists of a primary transmitter T and a primary receiver X. All nodes are equipped with a single antenna.[1]

[1]We note that the joint BPC and RIS phase configuration results are not available even for a single-antenna system and extension to multiple antennas is a good avenue for future work.

Authorized licensed use limited to: Indian Institute of Technology. Downloaded on November 03,2026 at 17:26:23 UTC from IEEE Xplore. Restrictions apply.

The complex baseband channel gains for direct S-D, S-X, and T-D links are denoted by h_{SD}, h_{SX}, and h_{TD}, respectively. We consider independent Rayleigh fading for these links. Therefore, $h_{SD} \sim \mathcal{CN}(0, \mu_{SD})$, $h_{SX} \sim \mathcal{CN}(0, \mu_{SX})$, and $h_{TD} \sim \mathcal{CN}(0, \mu_{TD})$ where μ_{SD}, μ_{SX}, and μ_{TD} denote their mean channel power gains, respectively.

We model the complex baseband channel gains between node A and node B following *spatially correlated Rician* fading, where A-B belongs to S-R, R-D, R-X, and T-R. Hence, the baseband channel gain vector is given as $\mathbf{h}_{AB} = \sqrt{\mu_{AB}}\left(\sqrt{K_{AB}/(1+K_{AB})}\bar{\mathbf{h}}_{AB} + \sqrt{\mathbf{C}/(1+K_{AB})}\tilde{\mathbf{h}}_{AB}\right)$, where K_{AB} denotes the Rician factor and μ_{AB} represents the mean channel power gain. Furthermore, $\bar{\mathbf{h}}_{AB}$ denotes the fixed channel gain vector associated with the line-of-sight (LoS) component, while $\tilde{\mathbf{h}}_{AB}$ denotes the non-LoS channel gain vector following independent $\mathcal{CN}(\mathbf{0}, \mathbf{I})$ distribution [2], [31]. Furthermore, $\mathbf{C}$ denotes the spatial correlation matrix of RIS-aided channel gains. The channel gains from (to) any node to (from) different RIS elements are correlated due to the rectangular geometry and depends on the size of the RIS element [29]. The spatial correlation between the m^{th} and n^{th} RIS elements with spacing d_{mn} is represented as

$$[\mathbf{C}]_{m,n} = \text{sinc}\left(\frac{2d_{mn}}{\lambda}\right), \quad \text{for } m, n = [1, 2, \ldots, M], \quad (1)$$

where $\text{sinc}(x) = \sin(\pi x)/(\pi x)$ [29].

Let $\theta_{h_{SX}}$, $\theta_{h_{SD}}$, $\theta_{h^m_{SR}}$, $\theta_{h^m_{RD}}$, $\theta_{h^m_{RX}}$ denote the phases of the corresponding baseband channel gains h_{SX}, h_{SD}, h^m_{SR}, h^m_{RD}, and h^m_{RX}, for $1 \leq m \leq M$, respectively. The RIS reflection coefficient can be expressed as $\Phi_m = \beta_m e^{j\theta_m}$, where $\beta_m \in [0, 1]$ and $\theta_m \in [0, 2\pi)$ is the reflection loss and the phase shift induced by the m^{th} RIS element, respectively. To maximize the reflection power of the RIS, we fix $\beta_m = 1$, for all m, as typically considered in [11], [17], and [19]. Let $\mathbf{\Theta} \triangleq [\theta_1, \theta_2, \ldots, \theta_M]$ denote the RIS phase shift vector.

A. Signal and Interference Model

We assume that S sends a data symbol x to D, where $\mathbb{E}[|x^2|] = 1$. According to a *binary power control* policy, $P_S \in \{P_{\max}, 0\}$ represents the transmit power of S. By it, when S is on, it transmits with the peak power $P_{\max}$ and when it is off, the transmit power is zero. We assume quasi-static and flat-fading channel model. Furthermore, the RIS is always assumed to be on during data transmission from S to D. The combined received signal at D through the direct link and RIS-reflected link is given by

$$y_D = \sqrt{P_S}\left(h_{SD} + \sum_{m=1}^{M} h^m_{RD} e^{j\theta_m} h^m_{SR}\right) x + n_D + n_P, \quad (2)$$

where, $n_D \sim \mathcal{CN}(0, \sigma_D^2)$ is the Gaussian noise at D and n_P is the combined interference signal received at D from T.

Interference from T to D: The following are the two widely considered interference power models in the literature from T.

- *Instantaneous Interference Power Model [11]:* In this model, combined interference power from T to D is given by $|n_P|^2 = P_T \left| h_{TD} + \sum_{m=1}^{M} h^m_{RD} e^{j\theta_m} h^m_{TR} \right|^2$, where P_T is the fixed transmit power of T. The SINR at D as a function of P_S and $\mathbf{\Theta}$ is then expressed as $\gamma_S(P_S, \mathbf{\Theta}) = P_S \left| h_{SD} + \sum_{m=1}^{M} h^m_{RD} e^{j\theta_m} h^m_{SR} \right|^2 \Big/ \left(\sigma_D^2 + |n_P|^2\right)$.
- *Average Interference Power Model [9], [32]:* This model instead considers the average interference power from T to D, which is given by $\mathbb{E}\left[|n_P|^2\right] = P_T \mathbb{E}\left[\left| h_{TD} + \sum_{m=1}^{M} h^m_{RD} e^{j\theta_m} h^m_{TR} \right|^2\right]$, and then writes the SINR at D as a function of P_S and $\mathbf{\Theta}$ as $\gamma_S(P_S, \mathbf{\Theta}) = P_S \left| h_{SD} + \sum_{m=1}^{M} h^m_{RD} e^{j\theta_m} h^m_{SR} \right|^2 \Big/ \left(\sigma_D^2 + \mathbb{E}\left[|n_P|^2\right]\right)$. We note that the denominator of $\gamma_S(P_S, \mathbf{\Theta})$ in the average interference power model depends only on the mean channel power gains μ_{TD}, μ_{TR}, and μ_{RD}, and not on their instantaneous channel states.

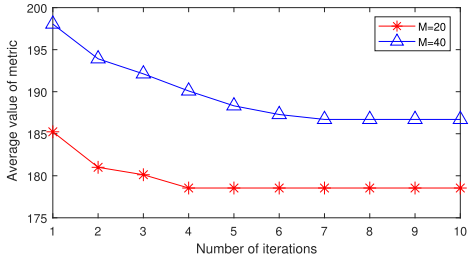


Fig. 2. Convergence of the CDA algorithm.

Remark 1: The choice of $\mathbf{\Theta}$ for the instantaneous interference power model impacts both the numerator and denominator of $\gamma_S(P_S, \mathbf{\Theta})$. However, in the average interference power model, $\mathbf{\Theta}$ impacts only the numerator term. For analytical tractability and to gain insights, we consider the average interference power model. The SEP using the two interference power models shall be compared in Fig. 11a.[2]

Interference from S to X: The interference signal received at X due to transmissions by S via direct link and RIS-reflected link is $\sqrt{P_S}\left(h_{SX} + \sum_{m=1}^{M} h^m_{RX} e^{j\theta_m} h^m_{SR}\right) x$. Therefore, instantaneous interference power at X as a function of P_S and $\mathbf{\Theta}$ can be written as

$$I(P_S, \mathbf{\Theta}) = P_S \left| h_{SX} + \sum_{m=1}^{M} h^m_{RX} e^{j\theta_m} h^m_{SR} \right|^2. \quad (3)$$

An *average interference constraint* is imposed on S by the primary system. It states that the fading-averaged interference power at X due to transmissions by S is less than or equal to a threshold I_{th}, i.e., $\mathbb{E}[I(P_S, \mathbf{\Theta})] \leq I_{\text{th}}$.[3]

[2]Our model is more practical than [12], [19], and [31], where the interference from T to D is neglected assuming that T is far from the secondary system.

[3]This is less restrictive than the peak interference constraint and can handle noisy channel estimates. It is appropriate when packet transmission duration of the primary system is typically larger than the coherence time of the S-to-X channel. Therefore, primary transmissions last long enough to average over multiple coherence intervals. Otherwise, the constraint is well-suited when the primary system delivers non-real-time applications and internet services such as browsing, email, and file exchange [9].

Authorized licensed use limited to: Indian Institute of Technology. Downloaded on November 03,2026 at 17:26:23 UTC from IEEE Xplore. Restrictions apply.

B. Problem Statement

Our objective is to minimize the average SEP of the secondary system. Let SEP(γ_S) denote the instantaneous SEP at D, which is a function of received SINR γ_S. From [30, (14)], for many modulation schemes, it can be approximated to the following closed form SEP(γ_S) $\approx c_1 \exp(-c_2\gamma_S)$, where c_1 and c_2 are modulation dependent constants. Our goal is to jointly optimize source's transmit power $P_S \in \{P_{\max}, 0\}$ and the RIS phase shift vector $\boldsymbol{\Theta}$ in order to minimize the average SEP of the secondary system subject to the average interference constraint. To keep the notation simple, we do not explicitly show the dependence of P_S and $\boldsymbol{\Theta}$ on the various channel fades. The optimization problem $\mathcal{P}$ is formulated as

$$\mathcal{P}: \min_{P_S,\boldsymbol{\Theta}} \ \mathbb{E}[c_1 \exp(-c_2\gamma_S(P_S,\boldsymbol{\Theta}))], \tag{4}$$

$$\text{s.t.} \ \ \mathbb{E}[I(P_S,\boldsymbol{\Theta})] \le I_{\text{th}}, \tag{5}$$

$$P_S \in \{P_{\max}, 0\}. \tag{6}$$

III. Optimal BPC and RIS Passive Beamforming

We now systematically derive an *optimal rule* for joint BPC at S and passive beamforming at the RIS that solves $\mathcal{P}$. Let $\bar{P}_S$ denote the optimal transmit power of S and $\bar{\boldsymbol{\Theta}} = [\bar{\theta}_1, \bar{\theta}_2, \ldots, \bar{\theta}_M]$ denote the optimal phase shift vector of the RIS reflective elements. A feasible rule is the one that satisfies the average interference constraint in (5). We have to find $\bar{P}_S$ and $\bar{\boldsymbol{\Theta}}$ that minimizes the average SEP at D while satisfying the average interference constraint at X. Let SEP$(P_S,\boldsymbol{\Theta}) = c_1\exp(-c_2\gamma_S(P_S,\boldsymbol{\Theta}))$ denote the instantaneous SEP for any P_S and $\boldsymbol{\Theta}$. Further, I_{un} denotes the average interference power at X when RIS phase shifts and transmit power of S is set to obtain the minimum average SEP at D when no interference constraint is active, i.e., $I_{\text{th}} = \infty$. It happens when $P_S = P_{\max}$ and $\theta_m = \theta_{h_{SD}} - (\theta_{h_{SR}^m} + \theta_{h_{RD}^m})$, for $1 \le m \le M$. Depending on the value of I_{un} relative to I_{th}, the optimal rule can be characterised as follows:

- *Region I ($I_{\text{un}} \le I_{\text{th}}$)*: The optimal values of P_S and $\boldsymbol{\Theta}$ that minimizes the average SEP at D while satisfying the average interference constraint is given by

$$\bar{P}_S = P_{\max} \text{ and } \bar{\boldsymbol{\Theta}} = \boldsymbol{\theta}_{h_{SD}}\mathbf{1} - (\boldsymbol{\Theta}_{h_{SR}} + \boldsymbol{\Theta}_{h_{RD}}), \tag{7}$$

  where $\boldsymbol{\Theta}_{h_{SR}} \triangleq \left[\theta_{h_{SR}^1}, \theta_{h_{SR}^2}, \ldots, \theta_{h_{SR}^M}\right]$, $\boldsymbol{\Theta}_{h_{RD}} \triangleq \left[\theta_{h_{RD}^1}, \theta_{h_{RD}^2}, \ldots, \theta_{h_{RD}^M}\right]$, and $\mathbf{1} \triangleq [1, 1, \ldots, 1]$. We shall refer the rule in (7) as the *unconstrained rule* henceforth. The average interference caused by it is equal to I_{un} and shall be analyzed in Section V.
- *Region II ($I_{\text{un}} > I_{\text{th}}$)*: The unconstrained rule is not a feasible rule in this region as the average interference caused by it is more than the interference threshold. Therefore, it cannot be optimal. The following result completely characterizes the optimal rule in this region.

Result 1: The optimal BPC and RIS beamforming rule that minimizes the average SEP under the average interference constraint in Region II is

$$(\bar{P}_S, \bar{\boldsymbol{\Theta}}) = \underset{P_S,\boldsymbol{\Theta}}{\text{argmin}} \{\text{SEP}(P_S,\boldsymbol{\Theta}) + \delta I(P_S,\boldsymbol{\Theta})\}. \tag{8}$$

Algorithm 1 Algorithm to Obtain Optimal δ and $(\bar{P}_S, \bar{\boldsymbol{\Theta}})$

1: **Initialize** $\delta = \delta_l = \delta_u = 0$
2: Compute $I_{\text{avg}}(\delta) = \mathbb{E}[I(\bar{P}_S, \bar{\boldsymbol{\Theta}})]$. Until $I_{\text{avg}}(\delta) \le I_{\text{th}}$, find δ_u by updating $\delta_u \leftarrow \delta + 0.01$ and obtaining $(\bar{P}_S, \bar{\boldsymbol{\Theta}})$ using (8) for $\delta = \delta_u$.
3: **while** $|I_{\text{avg}}(\delta) - I_{\text{th}}| > \epsilon$ **do**
4: Calculate $\delta = \frac{\delta_l + \delta_u}{2}$. Find $(\bar{P}_S, \bar{\boldsymbol{\Theta}})$ by using (8).
5: Compute $I_{\text{avg}}(\delta) = \mathbb{E}[I(\bar{P}_S, \bar{\boldsymbol{\Theta}})]$.
6: If $I_{\text{avg}}(\delta) < I_{\text{th}}$, $\delta_l \leftarrow \delta$; otherwise $\delta_u \leftarrow \delta$.
7: **end while**
8: **return** The optimal solutions for δ and $(\bar{P}_S, \bar{\boldsymbol{\Theta}})$.

In this region, we have $\delta > 0$. The value of δ is computed such that the secondary system satisfies the average interference constraint with *equality*. Therefore,

$$I_{\text{avg}}(\delta) \triangleq \mathbb{E}[I(\bar{P}_S, \bar{\boldsymbol{\Theta}})] = I_{\text{th}}. \tag{9}$$

Proof: The proof is relegated to Appendix A. ■

Insights into the behaviour of the optimal rule are as follows:

i) We shall refer to SEP$(P_S,\boldsymbol{\Theta}) + \delta I(P_S,\boldsymbol{\Theta})$ in (8) as the *metric*. The optimal rule finds the transmit power and the IRS phase shifts that minimize it. In it, the first term is the instantaneous SEP at D and the second term is the instantaneous interference power at X weighted by an *interference penalty factor* δ. The metric is equal to c_1 when $P_S = 0$, i.e., S is off. So the optimal rule first minimizes SEP$(P_{\max},\boldsymbol{\Theta}) + \delta I(P_{\max},\boldsymbol{\Theta})$ to obtain $\bar{\boldsymbol{\Theta}}$. Then, if SEP$(P_{\max},\bar{\boldsymbol{\Theta}}) + \delta I(P_{\max},\bar{\boldsymbol{\Theta}}) < c_1$, the optimal rule configures $\bar{\boldsymbol{\Theta}}$ at the RIS and transmits with $P_S = P_{\max}$. Otherwise, it chooses $P_S = 0$ to control the interference.

ii) For $\delta = 0$, the metric reduces to SEP$(P_S,\boldsymbol{\Theta})$. As SEP is a monotonically decreasing function of $\gamma_S(P_S,\boldsymbol{\Theta})$, the optimal rule becomes equivalent to the unconstrained rule in (7) and the average interference is equal to I_{un}.

iii) *Existence and Obtaining δ:* Note that $I_{\text{avg}}(0) = I_{\text{un}}$ and we can show that $I_{\text{avg}}(\delta)$ is a continuous and monotonically decreasing function of δ from I_{un} to zero, for $\delta > 0$. Hence, for $I_{\text{un}} > I_{\text{th}}$, an unique δ exists such that $I_{\text{avg}}(\delta) = I_{\text{th}}$. It can be obtained using bisection search. Therefore, the average interference power caused to X by the optimal rule is given by $\min\{I_{\text{th}}, I_{\text{un}}\}$. The algorithm to compute optimal δ and $(\bar{P}_S, \bar{\boldsymbol{\Theta}})$ is summarized in Algorithm 1.

Obtaining $\bar{\boldsymbol{\Theta}}$ with $P_S = P_{\max}$ in Region II: For $P_S = P_{\max}$, by taking partial derivative of the metric SEP$(P_{\max},\boldsymbol{\Theta}) + \delta I(P_{\max},\boldsymbol{\Theta})$ w.r.t. θ_m, and setting it to zero, we get the following equation for $1 \le m \le M$:

$$a_m Y_m + a_m^* Y_m^* + \sum_{l=1 l\neq m}^{M} C_{ml} Y_m Y_l^* + C_{ml}^* Y_m^* Y_l = \frac{c_1 c_2}{\delta\sigma^2} \exp\left(-\frac{c_2 P_{\max}}{\sigma^2}\left|h_{SD} + \sum_{m=1}^{M} h_{RD}^m Y_m h_{SR}^m\right|^2\right)(b_m Y_m + b_m^* Y_m^* + \sum_{l=1 l\neq m}^{M} D_{ml} Y_m Y_l^* + D_{ml}^* Y_m^* Y_l),$$

where $a_m = j h_{SR}^m h_{RX}^m h_{SX}^*$, $b_m = j h_{SR}^m h_{RD}^m h_{SD}^*$, $C_{ml} = j h_{SR}^m h_{RX}^m h_{SR}^{l^*} h_{RX}^{l^*}$, $D_{ml} = j h_{SR}^m h_{RD}^m h_{SR}^{l^*} h_{RD}^{l^*}$, and $Y_m = e^{j\theta_m}$. Obtaining $\bar{\boldsymbol{\Theta}}$ for the optimal rule involves solving a system of M non-linear equations with M unknowns, and its computational complexity is analyzed in Section IV-C.

Authorized licensed use limited to: Indian Institute of Technology. Downloaded on November 03,2026 at 17:26:23 UTC from IEEE Xplore. Restrictions apply.

Low Complexity Implementation: We next propose a low-complexity coordinate descent algorithm (CDA) to obtain RIS phases. At each iteration of CDA, we first minimise the metric w.r.t. one phase shift θ_m while the other phase shifts are kept fixed. It requires $\mathcal{O}(M)$ computations per iteration as we need to solve for M phase shifts one by one. Fig. 2 shows the convergence plot of the CDA for different values of M. We plot the average value of the metric as a function of the CDA iteration index. We observe that 4 iterations are enough for the convergence of the metric with $M = 20$. As M increases, more iterations are needed.

IV. Low-Complexity Rules

We next propose two low-complexity rules; i) Low interference (LI) rule and ii) Maximum signal power (MSP) rule for joint BPC and RIS beamforming under the average interference constraint.

A. Low Interference (LI) Rule

When S transmits with power $P_S = P_{\max}$, the primary receiver will experience lower interference when the direct S-X link is 180° out of phase with the composite S-RIS-X link. Therefore, the LI rule sets $\theta_m = \pi + \theta_{h_{SX}} - \left(\theta_{h_{SR}^m} + \theta_{h_{RX}^m}\right)$, for $1 \leq m \leq M$. From (3), the equivalent channel power gain from S to X denoted by $g_{\text{LI}} = I(P_S, \boldsymbol{\Theta})/P_S$. It is given by

$$g_{\text{LI}} = \left(|h_{SX}| - \sum_{m=1}^{M} |h_{RX}^m||h_{SR}^m| \right)^2. \tag{10}$$

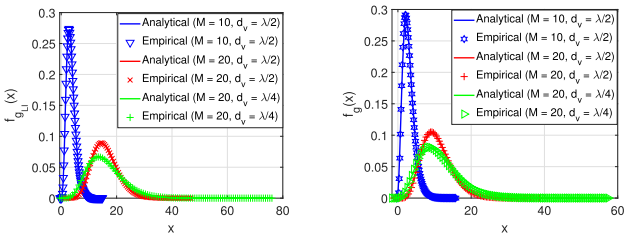
Power Control for LI Rule: We use the following BPC policy for the LI rule. If $P_{\max}\mathbb{E}[g_{\text{LI}}] \leq I_{\text{th}}$, then $P_S = P_{\max}$. Else let, $\alpha > 0$ is the unique solution of the equation

$$P_{\max} \int_0^{\alpha} x f_{g_{\text{LI}}}(x)\, dx = I_{\text{th}}, \tag{11}$$

where $f_{g_{\text{LI}}}(x)$ denotes the PDF of g_{LI}. Then, the power is given by $P_S = P_{\max}$, if $g_{\text{LI}} \leq \alpha$; otherwise, $P_S = 0$. Therefore, the LI rule transmits with power $P_{\max}$ when interference channel power gain is below a threshold. Otherwise, it chooses zero power option. We note that for independent RIS channel gains, the exact PDF of g_{LI} is given by [23, (13)]. Under correlated channels, the PDF of g_{LI} can be moment matched to a Gamma distributed random variable (RV) as

$$f_{g_{\text{LI}}}(x) = \frac{x^{\kappa-1} e^{-\frac{x}{\varpi}}}{\Gamma(\kappa)\varpi^{\kappa}}, \quad x > 0, \tag{12}$$

where $\kappa = \left(\mathbb{E}[g_{\text{LI}}]\right)^2 / \text{Var}(g_{\text{LI}})$ and $\varpi = \text{Var}(g_{\text{LI}})/\mathbb{E}[g_{\text{LI}}]$ denote the shape and scale parameters, respectively. The derivation for $\mathbb{E}[g_{\text{LI}}]$ is provided in Section V. To compute the variance, we obtain $\mathbb{E}\left[g_{\text{LI}}^2\right]$ numerically. The accuracy of the PDF of g_{LI} is verified in Fig. 3a by plotting analytical PDF and empirical PDF for different number of RIS elements M and RIS element spacing d_v. We show that our analytical PDF matches with that obtained from the simulations.



(a) PDF of g_{LI} (b) PDF of g

Fig. 3. PDF of g_{LI} and g for different M and d_v.

Computing α: Substituting (12) in (11) and simplifying further, we get the following equation $\gamma(\kappa+1, \alpha/\varpi) = I_{\text{th}}\Gamma(\kappa)/(\varpi P_{\max})$, where $\gamma(.,.)$ is the lower incomplete Gamma function [33]. Solving this equation numerically yields the threshold α that satisfies the interference constraint.

Average Interference: The average interference power caused to X by the LI rule is $\min\{I_{\text{th}}, P_{\max}\mathbb{E}[g_{\text{LI}}]\}$.

B. Maximum Signal Power (MSP) Rule

When S transmits with power $P_S = P_{\max}$, the received signal power at D will be the maximum when the direct S-D link is in phase with the composite S-RIS-D link. Therefore, the MSP rule sets $\theta_m = \theta_{h_{SD}} - \left(\theta_{h_{SR}^m} + \theta_{h_{RD}^m}\right)$, for $1 \leq m \leq M$. In this case, the equivalent channel power gain from S to X, which is denoted by g, is given by

$$g = \left| h_{SX} + e^{j\theta_{h_{SD}}} \sum_{m=1}^{M} |h_{RX}^m||h_{SR}^m| e^{j\left(\theta_{h_{RX}^m} - \theta_{h_{RD}^m}\right)} \right|^2. \tag{13}$$

Power Control for MSP Rule: We use the following BPC policy for the MSP rule. Let the average interference power at X caused by the MSP rule's phase shift choice is $I_{\text{un}} \triangleq P_{\max}\mathbb{E}[g]$. If $I_{\text{un}} \leq I_{\text{th}}$, then $P_S = P_{\max}$. Else Let $\beta > 0$ is the unique solution of $P_{\max} \int_0^{\beta} x f_g(x)\, dx = I_{\text{th}}$, where $f_g(x)$ denotes the PDF of g. Then, the MSP rule uses the following power control policy: $P_S = P_{\max}$, if $g \leq \beta$; otherwise, $P_S = 0$. The PDF of g can be moment matched to Gamma RV as given in (12), where $\mathbb{E}[g] = I_{\text{un}}/P_{\max}$ with I_{un} is derived later in (27) and $\mathbb{E}\left[g^2\right]$ is obtained numerically for evaluating $\text{Var}(g)$. The accuracy of the PDF of g is verified in Fig. 3b by plotting analytical PDF and empirical PDF. We show that our analytical PDF matches with that obtained from the simulations for different values of M and d_v. Using the PDF of g, the parameter β can obtained by solving the equation $\gamma(\kappa+1, \beta/\varpi) = I_{\text{th}}\Gamma(\kappa)/(\varpi P_{\max})$.

Average Interference: The average interference power caused to X by the MSP rule is given by $\min\{I_{\text{th}}, I_{\text{un}}\}$.

Discussion on CSI Assumptions: Channel estimation is necessary for implementing the proposed optimal rule, LI rule, and MSP rules. Considering the passive nature of the RIS, we adopt the time-division duplex protocol to exploit channel reciprocity and reduce CSI feedback overhead. Following the channel estimation protocol in [2], S needs to know perfect knowledge about the direct S-D channel gain h_{SD} and the cascaded channel gain matrix $\mathbf{H}_{RD}\mathbf{h}_{SR}$ of S-RIS-D link,

Authorized licensed use limited to: Indian Institute of Technology. Downloaded on November 03,2026 at 17:26:23 UTC from IEEE Xplore. Restrictions apply.

TABLE II
COMPLEXITY COMPARISON

Scheme	Pilots	Complexity
Optimal rule	$2(M+1)$	$\mathcal{O}(kM^3\log(1/\epsilon))$ or $\mathcal{O}(kM\log(1/\epsilon))$
LI rule	$M+1$	$\mathcal{O}(M)$
MSP rule	$M+1$	$\mathcal{O}(M)$

where $\mathbf{H}_{RD} = \text{diag}\,(\mathbf{h}_{RD})$, $\mathbf{h}_{RD} = [h_{RD}^1, \ldots, h_{RD}^M]^T$, and $\mathbf{h}_{SR} = [h_{SR}^1, \ldots, h_{SR}^M]^T$, whose details have been omitted for brevity. Furthermore, S can estimate the direct S-X channel gain h_{SX} and the cascaded channel gain matrix $\mathbf{H}_{RX}\mathbf{h}_{SR}$ of S-RIS-X link, where $\mathbf{H}_{RX} = \text{diag}\,(\mathbf{h}_{RX})$. This can be acquired either by a band manager or by pilot-based channel estimation techniques [23], [27]. The source computes $\boldsymbol{\Theta}$ based on this CSI and communicates to the RIS controller through a control link. The optimal rule developed under this allows us to obtain the average SEP lower bound for a scenario in the presence of imperfect CSI, as we shall show in Fig 15.

C. Computational Complexity Comparison

Optimal Rule: Obtaining optimal $\bar{\boldsymbol{\Theta}}$ for the optimal rule involves solving a system of M non-linear equations with M unknowns. Efficient multi-step iterative methods, such as Newton-Raphson's method that exhibits a quadratic convergence with $\mathcal{O}(kM^3)$ computations for k iterations or gradient descent method that has linear convergence with $\mathcal{O}(kM))$ computations can be employed [34]. For desired accuracy ϵ, the bisection search over δ incurs an additional logarithmic complexity, i.e., $\mathcal{O}(\log(1/\epsilon))$. Therefore, the total complexity associated with implementing the optimal rule is $\mathcal{O}\left(C_{\text{phase}}\ \log(1/\epsilon)\right)$, where $C_{\text{phase}} = \mathcal{O}\left(kM^3\right)$ for Newton-based method and $C_{\text{phase}} = \mathcal{O}(kM)$ for Gradient-based method. The optimal rule requires CSI of the both secondary links and secondary to primary interference links, which requires at least $2(M+1)$ pilots.

Both the LI and MSP rules use closed-form expressions to compute RIS phase shifts, which requires $\mathcal{O}(M)$ computations. The parameters α and β to control power are obtained by solving equations that depends only on the channel statistics that vary slowly compared to the instantaneous channel gains. Furthermore, both these low complexity rules requires only $M+1$ pilots as they depend either only on secondary link channel gains or the interference link channel gains. Table II compares number of pilot transmissions and computational complexity of the proposed rules.

V. ANALYSIS OF AVERAGE INTERFERENCE POWER

We now derive closed-form expressions for the average interference power at X for the LI and MSP rules, separately, with $P_S = P_{\max}$.

A. Average Interference Power of the LI Rule

The instantaneous interference channel power gain corresponding to the LI rule is given by (10). Therefore, the instantaneous interference power at X when S transmits with power $P_S = P_{\max}$, is given by

$$I(P_S, \boldsymbol{\Theta}) = P_{\max}\left(|h_{SX}| - \sum_{m=1}^{M}|h_{RX}^m||h_{SR}^m|\right)^2. \quad (14)$$

Then, $I(P_S,\boldsymbol{\Theta})/P_{\max} = |h_{SX}|^2 + \left(\sum_{m=1}^{M}|h_{RX}^m||h_{SR}^m|\right)^2 - 2|h_{SX}|\sum_{m=1}^{M}|h_{RX}^m||h_{SR}^m|$. We now derive the fading averaged interference power of the LI rule in the following Result.

Result 2: The lower average interference power $I_{\text{avg}}^{\text{low}}$ at X when $P_S = P_{\max}$ and $\theta_m = \pi + \theta_{h_{SX}} - \left(\theta_{h_{SR}^m} + \theta_{h_{RX}^m}\right)$, for $1 \le m \le M$, is given by

$$I_{\text{avg}}^{\text{low}} = \mathbb{E}[I(P_S,\boldsymbol{\Theta})] = A_1 + A_2 - A_3. \quad (15)$$

where,

$$A_1 = P_{\max}\mu_{SX}, \quad (16)$$

$$A_3 = P_{\max}M\sqrt{\frac{\pi^3\mu_{SX}\mu_{SR}\mu_{RX}}{16\,(K_{RX+1})(K_{SR+1})}}L_{\frac{1}{2}}(-K_{SR})\,L_{\frac{1}{2}}(-K_{RX}), \quad (17)$$

$$A_2 = P_{\max}M\mu_{SR}\mu_{RX} + P_{\max}\sum_{m=1}^{M}\sum_{\substack{n=1\\n\neq m}}^{M}\mathbb{E}\left[|h_{RX}^m|\,|h_{RX}^n|\right]\mathbb{E}\left[|h_{SR}^m|\,|h_{SR}^n|\right], \quad (18)$$

with

$$\begin{aligned}\mathbb{E}\left[|h_{\mathcal{XY}}^m||h_{\mathcal{XY}}^n|\right] &= D_{\mathcal{XY}}\sum_{q=0}^{\infty}\varepsilon_q\sum_{a,b,c=0}^{\infty}\frac{A_{\mathcal{XY}}(a,q)\,B_{\mathcal{XY}}(b,q)}{a!b!c!\,(a+q)!\,(b+q)!}\\ &\times\frac{C_{\mathcal{XY}}(c,q)}{(c+q)!}\Gamma\left(a+b+q+\frac{3}{2}\right)\Gamma\left(a+c+q+\frac{3}{2}\right)\\ &\times\frac{1}{4}\left[\left(1-\rho_{m,n}^2\right)2\sigma_{\mathcal{XY}}^2\right]^{2a+2q+b+c+3}, \end{aligned} \quad (19)$$

$D_{\mathcal{XY}} = \exp\left(-\frac{\nu_{SR}^2(1-\rho_{m,n})}{(1-\rho_{m,n}^2)\sigma_{\mathcal{XY}}^2}\right)/\left(1-\rho_{m,n}^2\right)\sigma_{\mathcal{XY}}^4$, $A_{\mathcal{XY}}(a,q) = \left(\frac{\rho_{m,n}}{2\left(1-\rho_{m,n}^2\right)\sigma_{\mathcal{XY}}^2}\right)^{2a+q}$, $B_{\mathcal{XY}}(b,q) = \left(\frac{\nu_{\mathcal{XY}}(1-\rho_{m,n})}{2\left(1-\rho_{m,n}^2\right)\sigma_{\mathcal{XY}}^2}\right)^{2b+q}$, $C_{\mathcal{XY}}(c,q) = \left(\frac{\nu_{\mathcal{XY}}(1-\rho_{m,n})}{2\left(1-\rho_{m,n}^2\right)\sigma_{\mathcal{XY}}^2}\right)^{2c+q}$, $2\sigma_{\mathcal{XY}}^2 = \frac{\mu_{\mathcal{XY}}}{(1+K_{\mathcal{XY}})}$, $\nu_{\mathcal{XY}}^2 = \frac{\mu_{\mathcal{XY}}K_{\mathcal{XY}}}{(1+K_{\mathcal{XY}})}$, for $\mathcal{XY} \in \{SR, RX\}$, $\rho_{m,n} = [\mathbf{C}]_{m,n}$, $\mathbf{C}$ denotes the spatial correlation matrix, ε_q is the Neumann factor such that $\varepsilon_0 = 1$ and $\varepsilon_q = 2$, for $q > 0$, $L_{1/2}(.)$ denotes the Laguerre polynomial of order $1/2$ [35, (22.2.13)], and $\Gamma(.)$ denotes the Gamma function [35, (6.1.1)].

Proof: The proof is relegated to Appendix B. ■

Interpretation: The term A_1 in (16) corresponds to the average interference due to the direct S-X link and is proportional to its average channel power gain μ_{SX}. The term A_2 in (18) corresponds to the average interference due to the cascaded S-RIS-X reflected link. It is proportional to the product of the average channel power gains μ_{SR} and μ_{RX}. The term A_3 in (17) corresponds to the average interference due to the combination of the direct and reflected interference links.

Authorized licensed use limited to: Indian Institute of Technology. Downloaded on November 03,2026 at 17:26:23 UTC from IEEE Xplore. Restrictions apply.

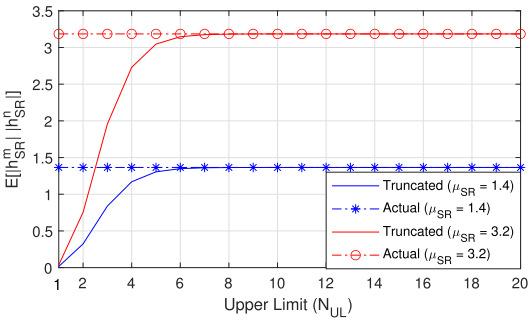


Fig. 4. $\mathbb{E}\left[|h_{SR}^m||h_{SR}^n|\right]$ as a function of upper limit N_{UL}.

Therefore, it is proportional to the product $\mu_{SX}\mu_{SR}\mu_{RX}$ and the number of IRS elements M. The subtraction of A_3 from $A_1 + A_2$ is due to the choice of phase shifts by the LI rule that combines direct and reflected links destructively.

Remark 2: From (18) and (19), we see that A_2 involves infinite summation terms. To reduce the number of computations, these infinite summations can be truncated using finite number of terms N_{UL}. To validate this, in Fig. 4, we have shown $\mathbb{E}[|h_{SR}^m||h_{SR}^n]\,|$ as a function of N_{UL} for two different values of μ_{SR}. We see that the truncated values with as small as 8 terms match well with the actual value.

Asymptotic Average Interference for Large M: To get more insights, we now derive the asymptotic expression for $I_{\mathrm{avg}}^{\mathrm{low}}$, for large values of M. Let $Y = \sum_{m=1}^{M} |h_{RX}^m|\,|h_{SR}^m|$ and $\mu_Y = \mathbb{E}[Y]$. Using [36, (47)], we can show that

$$\mu_Y = \tau \sum_{m=1}^{M} \sqrt{\mu_{SR}^m \mu_{RX}^m}, \tag{20}$$

where $\mu_{SR}^m = \mu_{SR} \sum_{n=1}^{M} \left|\left[\mathbf{C}^{1/2}\right]_{m,n}\right|^2$, $\mu_{RX}^m = \mu_{RX} \sum_{n=1}^{M} \left|\left[\mathbf{C}^{1/2}\right]_{m,n}\right|^2$, $\tau = \frac{\pi L_{1/2}(-K_{SR}) L_{1/2}(-K_{RX})}{4\sqrt{(K_{SR}+1)(K_{RX}+1)}}$. We note that the RVs $|h_{SR}^m|$ and $|h_{RX}^m|$ are independent and have finite mean and bounded variance. From (1), we can show that the covariances of $|h_{SR}^m|$ and $|h_{SR}^n|$, and also $|h_{RX}^m|$ and $|h_{RX}^n|$ tend to zero for $|m-n| \to \infty$. Therefore, under spatial correlation given in (1), for large M, it can be shown that [29, (21)]

$$\lim_{M\to\infty} \frac{1}{M} \sum_{m=1}^{M} |h_{SR}^m|\,|h_{RX}^m| \to \tau \sqrt{\mu_{SR}\mu_{RX}}. \tag{21}$$

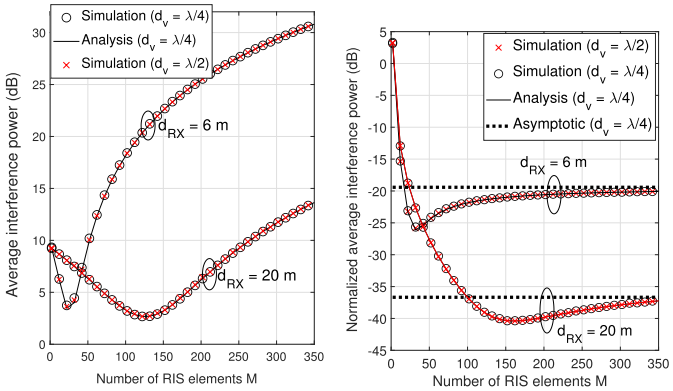
Using (21), we now derive the a closed-form expression for the normalized average interference power of the LI rule for large M.

Result 3: The lower average interference power normalized by M^2 under spatial correlation for large M is given by

$$\lim_{M\to\infty} \frac{I_{\mathrm{avg}}^{\mathrm{low}}}{M^2} \to \frac{P_{\max}\mu_{SX}}{M^2} + P_{\max}(\tau)^2 \mu_{SR}\mu_{RX} - \frac{P_{\max}}{M}\tau\sqrt{\pi\mu_{SR}\mu_{RX}\mu_{SX}}. \tag{22}$$

Proof: The proof is referred to Appendix C. ■

Insights: The first term in (22), is the average interference power due to the direct S-X link and increases linearly as $P_{\max}$ or μ_{SX} increases. The second term is due to the reflected



(a) $I_{\mathrm{avg}}^{\mathrm{low}}$ (b) $I_{\mathrm{avg}}^{\mathrm{low}}/M^2$

Fig. 5. $I_{\mathrm{avg}}^{\mathrm{low}}$ with and without normalization versus M when X is at different distances from the RIS and different values of RIS element spacing d_v ($d_{SR} = 98.5$m, $d_{SX} = 101.12$m, $P_{\max} = 10$ dBm, and $I_{\mathrm{th}}/\sigma_D^2 = 15$ dB).

S-RIS-X link and is proportional to the product $\mu_{SR}\mu_{RX}$, $P_{\max}$. The third term is due to the out of phase combination of the direct and reflected links. Therefore, it depends on the channel statistics of both direct and the reflected links. For sufficiently large M, we can show that the normalized average interference power saturates to the following constant independent of M as

$$\lim_{M\to\infty} \frac{I_{\mathrm{avg}}^{\mathrm{low}}}{M^2} \to P_{\max}(\tau)^2 \mu_{SR}\mu_{RX}. \tag{23}$$

Fig. 5(a) plots the average interference of the LI rule ($I_{\mathrm{avg}}^{\mathrm{low}}$) normalized with thermal noise power as a function of the number of RIS elements M. We see that the simulations match well with the analytical expression in (15). For low M, the average interference power due to the term A_3 in (15) that captures the out of phase combination of the signal from the direct and the reflected links dominates A_2. Therefore, as M increases, we observe that $I_{\mathrm{avg}}^{\mathrm{low}}$ initially decreases due to increased A_3. However, for large M, A_2 dominates A_3, which increases $I_{\mathrm{avg}}^{\mathrm{low}}$ as M increases. Note that as RIS-to-X distance d_{RX} increases, $I_{\mathrm{avg}}^{\mathrm{low}}$ reduces. We also see that the average interference power is independent of minimum inter-element spacing d_v for the RIS, which controls the channel correlation. Analysis is not shown for $d_v = \lambda/2$ to avoid clutter. Fig. 5(b) plots $I_{\mathrm{avg}}^{\mathrm{low}}/M^2$ normalized with thermal noise power as a function of M. The simulations match the analytical expression in (22) and the asymptotic expression in (23) track the analysis well for $M > 150$ with $d_{RX} = 6$ m. Further, the value of M at which the normalized average interference power reaches this constant is a function of d_{RX} and is independent of the channel correlation.

Special Case: For independent RIS-related channels gains, i.e., $|h_{SR}^m|$ is independent of $|h_{SR}^n|$, and $|h_{RX}^m|$ is independent of $|h_{RX}^n|$, for $n \neq m$, the term A_2 in (18) simplifies to A_2' as

$$A_2' = P_{\max} M \mu_{SR}\mu_{RX} + \frac{P_{\max} M\,(M-1)\,\pi^2 \mu_{SR}\mu_{RX}}{16\,(K_{SR}+1)\,(K_{RX}+1)} \times \left(L_{\frac{1}{2}}(-K_{SR}) L_{\frac{1}{2}}(-K_{RX})\right)^2. \tag{24}$$

The terms A_1 and A_3 remain the same as (16) and (17), respectively. Therefore, for the case of independent RIS-related

Authorized licensed use limited to: Indian Institute of Technology. Downloaded on November 03,2026 at 17:26:23 UTC from IEEE Xplore. Restrictions apply.

channels, $I_{\text{avg}}^{\text{low}}$ is given in closed-form as $I_{\text{avg}}^{\text{low}} = A_1 + A_2' - A_3$. For large M, this reduces to (22), and the same insights obtained from Fig. 5 apply here as well.

B. Unconstrained Average Interference Power ($I_{Th} = \infty$)

We now derive the average interference power I_{un} at X caused by the unconstrained rule. It is needed to obtain the average interference caused by the MSP rule, which is given by $\min\{I_{\text{th}}, I_{\text{un}}\}$. Expanding (3) and taking average over channel fades, we get unconstrained average interference power as

$$\begin{aligned} I_{\text{un}} &= P_{\max}\mathbb{E}\Bigg[|h_{SX}|^2 + h_{SX}^* \sum_{m=1}^{M} h_{RX}^m e^{j\theta_m} h_{SR}^m \\ &\quad + h_{SX} \sum_{m=1}^{M} \left(h_{RX}^m\right)^* e^{-j\theta_m} \left(h_{SR}^m\right)^* + \sum_{m=1}^{M} \left|h_{RX}^m\right|^2 \left|h_{SR}^m\right|^2 \\ &\quad + \sum_{m=1}^{M} \sum_{\substack{n=1 \\ n\neq m}}^{M} h_{RX}^m h_{SR}^m \left(h_{RX}^n\right)^* \left(h_{SR}^n\right)^* e^{j(\theta_m - \theta_n)}\Bigg], \\ &\triangleq T_1 + T_2 + T_3 + T_4 + T_5, \end{aligned} \tag{25}$$

where T_1 to T_5 are defined as the terms that appear in that order in (25).

From (25), we note that $T_1 = P_{\max}\mathbb{E}\left[|h_{SX}|^2\right] = P_{\max}\mu_{SX}$. The direct S-X channel gain h_{SX} is a zero mean RV, i.e., $\mathbb{E}[h_{SX}] = 0$. Furthermore, it is independent of the cascaded S-RIS-X link. Therefore, we get $T_2 = 0$ and $T_3 = 0$. Exploiting the independent channel property of S-RIS and RIS-X links, $T_4 = P_{\max}\mathbb{E}\left[\sum_{m=1}^{M} \left|h_{RX}^m\right|^2 \left|h_{SR}^m\right|^2\right] = MP_{\max}\mu_{SR}\mu_{RX}$. Substituting $\theta_m = \theta_{h_{SD}} - \left(\theta_{h_{SR}^m} + \theta_{h_{RD}^m}\right)$, we write T_5 as

$$\begin{aligned} T_5 &= P_{\max} \sum_{m=1}^{M} \sum_{\substack{n=1 \\ n\neq m}}^{M} \mathbb{E}\left[h_{RX}^m \left(h_{RX}^n\right)^*\right] \mathbb{E}\left[e^{j\left(\theta_{h_{RD}^n} - \theta_{h_{RD}^m}\right)}\right] \\ &\quad \times \mathbb{E}\left[\left|h_{SR}^m\right| \left|h_{SR}^n\right|\right]. \end{aligned} \tag{26}$$

We now simplify this expression in the following result.

Result 4: The unconstrained average interference power I_{un} at X when $P_S = P_{\max}$ and $\theta_m = \theta_{h_{SD}} - \left(\theta_{h_{SR}^m} + \theta_{h_{RD}^m}\right)$, for $1 \le m \le M$, is approximately given by

$$\begin{aligned} &I_{\text{un}} \\ &\approx P_{\max}\Bigg(\mu_{SX} + M\mu_{SR}\mu_{RX} + \sum_{m=1}^{M} \sum_{\substack{n=1 \\ n\neq m}}^{M} \Bigg[D_{SR} \sum_{q=0}^{N_{\text{UL}}} \varepsilon_q \\ &\times \sum_{a,b,c=0}^{N_{\text{UL}}} \frac{A_{SR}(a,q)\, B_{SR}(b,q)\, C_{SR}(c,q)}{a!b!c!\,(a+q)!\,(b+q)!\,(c+q)!} \Gamma\left(a+b+q+\frac{3}{2}\right) \\ &\times \Gamma\left(a+c+q+\frac{3}{2}\right) \frac{1}{4}\left[\left(1-\rho_{m,n}^2\right) 2\sigma_{SR}^2\right]^{2a+2q+b+c+3}\Bigg] \\ &\times \frac{(\rho_{m,n}+K_{RX})\mu_{RX}}{1+K_{RX}} \left[\sum_{q=0}^{\kappa} \sum_{p=0}^{\kappa} \sum_{i=1}^{N} w_i \int_{-\pi}^{\pi} e^{j\theta} \chi_{q,p}^{RD}(x_i,\theta) d\theta\right]\Bigg), \end{aligned} \tag{27}$$

where D_{SR}, $A_{SR}(a,q)$, $B_{SR}(b,q)$, $C_{SR}(c,q)$, and σ_{SR}^2 are defined in (19) and $\chi_{q,p}^{RD}(x_i,\theta)$ is defined later in (61).

Proof: The proof is referred to Appendix D. ■

Insights: We note that (27) involves computing finite summations and single-integral, which can be easily computed. As $P_{\max}$ increases, I_{un} increases. Among the three terms in (27), the first term is the average interference power due to the direct S-X link. It increases linearly as μ_{SX} increases. The second term represents the average interference power obtained via reflected S-RIS-X link, which is proportional to the product $\mu_{SR}\mu_{RX}$. The third term is the average interference power due to the phase combination of the signal from the direct and the reflected links. It depends on the direct and the reflected links channel statistics, correlation matrix $\mathbf{C}$, and Rician factors K_{SR}, K_{RX}, and K_{RD}.

Special Case: When RIS-related channels are *independent*, T_5 in (26) simplifies to

$$\begin{aligned} T_5 &= P_{\max} \sum_{m=1}^{M} \sum_{\substack{n=1 \\ n\neq m}}^{M} \mathbb{E}[h_{RX}^m]\, \mathbb{E}\left[\left(h_{RX}^n\right)^*\right] \mathbb{E}\left[e^{j\theta_{h_{RD}^n}}\right] \\ &\quad \times \mathbb{E}\left[e^{-j\theta_{h_{RD}^m}}\right] \mathbb{E}[|h_{SR}^m|]\, \mathbb{E}[|h_{SR}^n|]. \end{aligned} \tag{28}$$

Now, $\mathbb{E}[h_{RX}^m] = \sqrt{\mu_{RX} K_{RX}/(1+K_{RX})}$ and $\mathbb{E}[|h_{SR}^m|] = \sqrt{\pi\mu_{SR}/\left(4\left(K_{SR}+1\right)\right)} L_{1/2}\left(-K_{SR}\right)$. Further, using [37, (10)] and observing that the PDF of the phase θ under Rician fading model is an even function of θ, the term $\mathbb{E}\left[e^{j\theta}\right]$ simplifies to $\zeta(K)$ for Rician factor K, where $\zeta(K) = \sqrt{\frac{K}{\pi}} \int_0^{\pi} \cos^2\theta e^{-K\sin^2\theta}\left(1+\text{erf}\left(\sqrt{K}\cos\theta\right)\right) d\theta$ with erf (.) denotes the error function [35, (7.1.1)]. In (28), $K = K_{RD}$ for the RIS-D links. Therefore, we can show that

$$\begin{aligned} &T_5 \\ &= \frac{M(M-1)\, P_{\max}\pi\mu_{SR}\mu_{RX}K_{RX}\left(L_{1/2}(-K_{SR})\,\zeta(K_{RD})\right)^2}{4\left(K_{SR}+1\right)\left(K_{RX}+1\right)}. \end{aligned} \tag{29}$$

We note that T_1, T_2, T_3, and T_4 remain the same as in (25). Combining all the necessary terms yields the final expression for I_{un} with independent RIS-related channel gains as

$$\begin{aligned} I_{\text{un}} &= P_{\max}\Bigg(\mu_{SX} + M\mu_{SR}\mu_{RX} + \frac{M(M-1)\,\pi\mu_{SR}\mu_{RX}}{4\left(K_{SR}+1\right)\left(K_{RX}+1\right)} \\ &\quad \times K_{RX}\left(L_{1/2}(-K_{SR})\,\zeta(K_{RD})\right)^2\Bigg). \end{aligned} \tag{30}$$

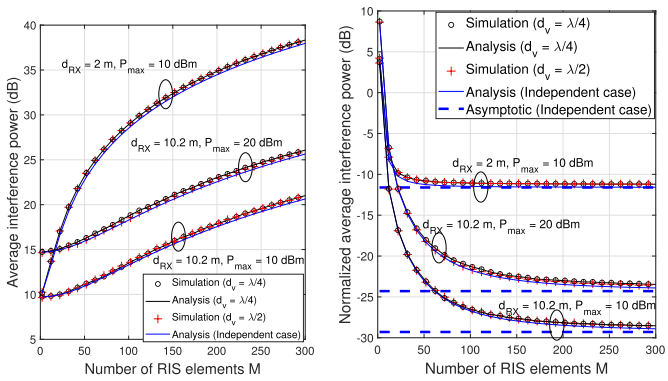
For large M, the I_{un}/M^2 saturates to the following constant independent of M as

$$\lim_{M\to\infty} \frac{I_{\text{un}}}{M^2} \to \frac{P_{\max}\pi\mu_{SR}\mu_{RX}K_{RX}\left(L_{1/2}(-K_{SR})\,\zeta(K_{RD})\right)^2}{4\left(K_{SR}+1\right)\left(K_{RX}+1\right)}. \tag{31}$$

This depends on system parameters $P_{\max}$, product of mean channel power gain $\mu_{SR}\mu_{RX}$, and Rician factors K_{SR}, K_{RX}, and K_{RD}.

Figs. 6a and 6b, respectively, plot I_{un} and I_{un}/M^2 in dB (normalized with thermal noise power) versus number of RIS elements M. Simulations results match well with analysis

Authorized licensed use limited to: Indian Institute of Technology. Downloaded on November 03,2026 at 17:26:23 UTC from IEEE Xplore. Restrictions apply.



(a) I_{un} (b) I_{un}/M^2

Fig. 6. I_{un} and I_{un}/M^2 versus no. of RIS elements M ($d_{SR} = 98.5$m, $d_{SX} = 101.9$m, and $I_{\text{th}}/\sigma_D^2 = 15$ dB).

obtained from (27). We see that as M increases, I_{un} monotonically increases, and I_{un}/M^2 decreases first and saturates at large M. We see only a marginal variation as d_v changes. We also plot the I_{un} obtained from analysis (c.f. (30)) for independent RIS-related channels and asymptotic value for I_{un}/M^2 as given in (31). We see a marginal increase in average interference power with correlation. Further, the average interference power increases as $P_{\max}$ increases or d_{RX} decreases, which is as expected.

Modeling Imperfect CSI: To investigate the robustness of our proposed schemes against channel estimation (CE) errors in practical scenarios, let $\hat{h}_{SX}$ and $\hat{h}_{SD}$ denote the channel estimates of the direct links h_{SX} and h_{SD}. Furthermore, let the cascaded link actual channel gains are denoted by $C_D^m = h_{SR}^m h_{RD}^m$ and $C_X^m = h_{SR}^m h_{RX}^m$, for $1 \le m \le M$. We can obtain an estimate of C_D^m, which we denote as $\hat{C}_D^m$, using orthogonal pilot sequences sent by the users [38]. Note that our proposed schemes require the knowledge of only the cascaded channel of the RIS, and thus can be implemented when the RIS is entirely passive. Moreover, estimating the direct links can be performed while the RIS is "switched off" (i.e. working in absorbing mode rather than reflecting mode). As a result, we employ four independent CE errors, two for the direct links, and two for the cascaded links as follows:

$$\hat{h}_{SX} = \sqrt{1-\sigma_I} h_{SX} + \sqrt{\sigma_I}\tilde{h}_{SX}, \tag{32}$$

$$\hat{h}_{SD} = \sqrt{1-\sigma_C} h_{SD} + \sqrt{\sigma_C}\tilde{h}_{SD}, \tag{33}$$

$$\hat{C}_D^m = \sqrt{1-\sigma_C} C_D^m + \sqrt{\sigma_C}\tilde{C}_D^m, \tag{34}$$

$$\hat{C}_X^m = \sqrt{1-\sigma_I} C_X^m + \sqrt{\sigma_I}\tilde{C}_X^m, \tag{35}$$

where $\tilde{h}_{SX}$, $\tilde{h}_{SD}$, and $\tilde{C}_D^m$, $\tilde{C}_X^m$ denote the corresponding CE errors of the direct link and cascaded link channel gains, respectively. They are modeled as complex Gaussian, independent of actual channel and having same statistics that of the actual channel gain. Moreover, $\sigma_I \in [0,1]$ and $\sigma_C \in [0,1]$ captures the estimation error for the S-X interference link and S-D communication link, respectively. We shall evaluate the impact of imperfect CSI on both the average interference power at X and on the average SEP performance at D in Fig. 15.

Alternate Scattering Matrix-based Correlation Model: We now consider a physically-consistent RIS model that explicitly accounts for mutual coupling effects, following [39] and [40]. In this framework, the RIS phase shift matrix is no longer modeled as a diagonal matrix, but instead as

$$\mathbf{\Psi} = \left(\mathbf{\Upsilon}^{-1} - \mathbf{S}\right)^{-1}, \tag{36}$$

where $\mathbf{\Upsilon} = \text{Diag}(\Phi_1, \Phi_2, \ldots, \Phi_m) \in \mathbb{C}^{M\times M}$ denotes the ideal diagonal phase shift matrix with unit-modulus elements with$\Phi_m = \beta_m e^{j\theta_m}$, where $\beta_m \in [0,1]$ and $\theta_m \in [0, 2\pi)$ is the reflection loss and the phase shift induced by the m^{th} RIS element, respectively. Furthermore, $\mathbf{S}$ represents the multi-port scattering matrix capturing the mutual coupling between the RIS elements. The above expression can be expanded using a Neumann series as

$$\left(\mathbf{\Upsilon}^{-1} - \mathbf{S}\right)^{-1} = \sum_{l=0}^{\infty} (\mathbf{\Upsilon}\mathbf{S})^l \mathbf{\Upsilon} = \mathbf{\Upsilon} + \mathbf{\Upsilon}\mathbf{S}\mathbf{\Upsilon} + \cdots, \tag{37}$$

which clearly reveals the contribution of higher-order reflections caused by mutual coupling. The scattering matrix $\mathbf{S}$ is constructed based on the embedded element pattern coupling matrix $\mathbf{B}$, whose entries depend on the spatial configuration of RIS elements. The (i,j)-th entry of $\mathbf{B}$ is expressed as

$$[\mathbf{B}]_{i,j} = \begin{cases} \dfrac{\pi a^2}{\lambda^2}, & i = j, \\ \dfrac{a}{\lambda}\dfrac{J_1\left(\frac{2\pi a}{\lambda} d_{i,j}\right)}{d_{i,j}}, & i \ne j, \end{cases} \tag{38}$$

where a denotes the inter-element spacing, λ is the wavelength, $d_{i,j}$ is the distance between elements, and $J_1(\cdot)$ is the first-order Bessel function. Based on the eigenvalue decomposition of $\mathbf{B}$, the scattering matrix $\mathbf{S}$ is obtained as

$$\mathbf{S} = \mathbf{U}\sqrt{\mathbf{I_M} - \mathbf{\Lambda}}\,\mathbf{U}^T, \tag{39}$$

where $\mathbf{\Lambda}$ is a diagonal matrix of eigenvalues of $\mathbf{B}$ and $\mathbf{U}$ contains the corresponding eigenvectors. Furthermore, the relationship between $\mathbf{B}$ and $\mathbf{S}$ satisfies

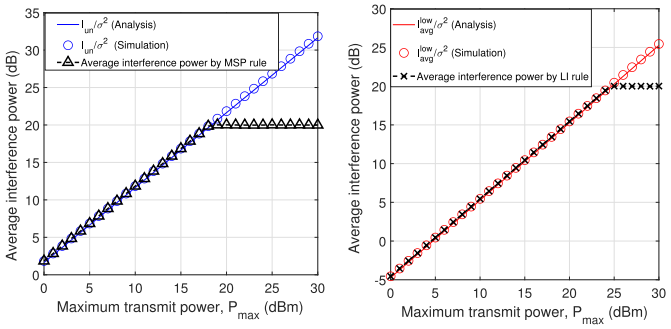
$$\mathbf{B} = \mathbf{I_M} - \mathbf{S}\mathbf{S}^H, \tag{40}$$

The impact of this alternate correlation model shall be demonstrated in Fig. 17.

VI. Numerical Results

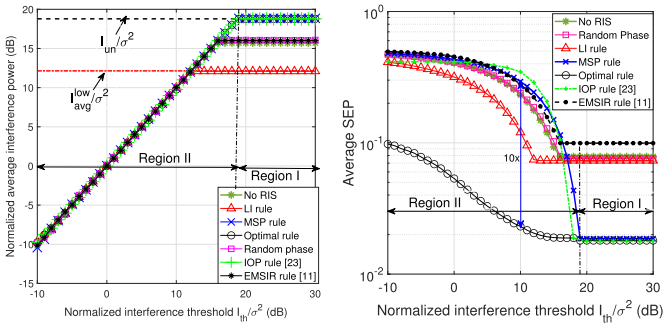
In this section, we now evaluate the performance of the proposed schemes using Monte Carlo simulations and validate analytical expressions. For any two nodes A $\in \{S, \text{RIS}\}$ and B $\in \{D, \text{RIS}, X\}$, the mean channel power gain by simplified path loss model is given by $\mu_{AB} = b_1 \left(d_0/d_{\text{AB}}\right)^{\varepsilon_{\text{AB}}}$ [19]. Here, $b_1 = -30$ dB denotes the path loss at a reference distance $d_0 = 1$ m, d_{AB} denotes the distance between the nodes A and B, and ε_{AB} denotes the path loss exponent, which is considered as 3.5 for the direct S-D and S-X channels and 2.5 for the RIS-assisted channels. We set the Rician factors as 2, and the sum of thermal noise power and mean interference power from T as $\sigma^2 = \sigma_D^2 + \mathbb{E}\left[|n_P|^2\right] = -100$ dBm. Unless mentioned otherwise, we set $d_{SD} = 100$ m,

Authorized licensed use limited to: Indian Institute of Technology. Downloaded on November 03,2026 at 17:26:23 UTC from IEEE Xplore. Restrictions apply.



(a) MSP Rule (b) LI Rule

Fig. 7. Average interference power by the LI and MSP rules versus $P_{\max}$ ($I_{\text{th}}/\sigma^2 = 20$ dB, $d_v = \lambda/4$, and $M = 10$).



(a) Average interference power (b) Average SEP

Fig. 8. Average interference power at X and average SEP at D as a function of I_{th}/σ^2 of various rules ($M = 20$, $P_{\max} = 15$ dBm, $d_v = \lambda/4$, and 8PSK).

$d_{SX} = 95.5$ m, $d_{SR} = 98.5$ m, $d_{RD} = 10.2$ m, $d_{RX} = 3$ m and carrier frequency $f_c = 2.4$ GHz and $\lambda = c/f_c$.

Average Interference Power at X: Figs. 7a and 7b plot the average interference power caused by the MSP and LI rules normalized with σ^2 in dB, respectively, as a function of $P_{\max}$ keeping I_{th}/σ^2 fixed at 20 dB. For reference, we also plot I_{un}/σ^2 and $I_{\text{avg}}^{\text{low}}/\sigma^2$ obtained both from simulation and analysis. We see that for low-to-mid $P_{\max}$, the normalized average interference power by the MSP rule and LI rule is I_{un}/σ^2 and $I_{\text{avg}}^{\text{low}}/\sigma^2$, respectively, and they increase linearly as $P_{\max}$ increases. However, for high $P_{\max}$, they saturate to $I_{\text{th}}/\sigma^2 = 20$ dB, hence satisfying the average interference constraint.

Performance Benchmarking: Figs. 8a and 8b plot the normalized average interference power at X, and the average SEP at D, respectively, for the optimal, LI, and MSP rules as a function of normalized interference threshold I_{th}/σ^2 for $P_{\max} = 15$ dBm. We now consider four benchmark schemes:

1. Interference-Outage Probability Constraint (IOP) Rule [23]: The optimal binary power control and RIS beamforming rule that minimizes the average SEP at D under an interference-outage constraint at X is given by [23]

$$\left(\bar{P}_S, \bar{\boldsymbol{\Theta}}\right) = \underset{P_S, \boldsymbol{\Theta}}{\operatorname{argmin}} \left\{ \text{SEP}\left(P_S, \boldsymbol{\Theta}\right) + \varkappa \mathbf{1}_{\{I(P_S,\boldsymbol{\Theta}) \geq I_{\text{th}}\}} \right\}, \tag{41}$$

where $\mathbf{1}_{\{a\}}$ denotes an indicator function; it is 1 if a is true and is 0 otherwise. In order to do a fair comparison with our scheme, the Lagrange parameter $\varkappa$ is chosen such that the average interference constraint is met with equality.

2. Enhanced Maximum Signal Power-to-Interference Power Ratio (EMSIR) Rule [11]: This rule selects the RIS phase shifts that maximizes the ratio between the S-D equivalent channel power gain to S-X equivalent interference channel power gain. Therefore, by this rule, the RIS phase shift vector $\boldsymbol{\Theta} \triangleq [\theta_1, \theta_2, \ldots, \theta_M]$ is obtained as

$$\bar{\boldsymbol{\Theta}} = \arg\max_{\boldsymbol{\Theta}} \frac{\left| h_{SD} + \sum_{m=1}^{M} h_{RD}^m e^{j\theta_m} h_{SR}^m \right|^2}{\left| h_{SX} + \sum_{m=1}^{M} h_{RX}^m e^{j\theta_m} h_{SR}^m \right|^2}. \tag{42}$$

For compact notations, we define $\mathbf{h}_{SRD} = \text{diag}\left(\mathbf{h}_{RD}\right) \mathbf{h}_{SR}$ and $\mathbf{h}_{SRX} = \text{diag}\left(\mathbf{h}_{RX}\right) \mathbf{h}_{SR}$, where $\mathbf{h}_{RD} = [h_{RD}^1, \ldots, h_{RD}^M]^T$, $\mathbf{h}_{RX} = [h_{RX}^1, \ldots, h_{RX}^M]^T$, and $\mathbf{h}_{SR} = [h_{SR}^1, \ldots, h_{SR}^M]^T$. Furthermore, we define $\overline{\mathbf{h}}_{SD} = [\mathbf{h}_{SRD}^T, h_{SD}]^T$, and $\overline{\mathbf{h}}_{SX} = [\mathbf{h}_{SRX}^T, h_{SX}]^T$.

We denote $\mathbf{H}_{SD} = \overline{\mathbf{h}}_{SD} \overline{\mathbf{h}}_{SD}^H$ and $\mathbf{H}_{SX} = \overline{\mathbf{h}}_{SX} \overline{\mathbf{h}}_{SX}^H$, $\mathbf{v}^H = [v_1, \ldots, v_M]$, $v_m = e^{j\theta_m}$, for $1 \leq m \leq M$, and $\overline{\mathbf{v}} = e^{j\omega}[\mathbf{v}^H, 1]$, where ω is an arbitrary phase rotation. Then, the equivalent channel power gains are given by $\left| h_{SD} + \sum_{m=1}^{M} h_{RD}^m e^{j\theta_m} h_{SR}^m \right|^2 = \overline{\mathbf{v}}^H \mathbf{H}_{SD} \overline{\mathbf{v}}$ and $\left| h_{SX} + \sum_{m=1}^{M} h_{RX}^m e^{j\theta_m} h_{SR}^m \right|^2 = \overline{\mathbf{v}}^H \mathbf{H}_{SX} \overline{\mathbf{v}}$ [11]. Using this, the EMSIR rule in (42) simplifies to

$$\bar{\boldsymbol{\Theta}} = \arg\max_{\boldsymbol{\Theta}} \frac{\overline{\mathbf{v}}^H \mathbf{H}_{SD} \overline{\mathbf{v}}}{\overline{\mathbf{v}}^H \mathbf{H}_{SX} \overline{\mathbf{v}}}. \tag{43}$$

The solution is obtained using the generalized Rayleigh quotient method by solving the vector $\overline{\mathbf{v}}$ to satisfy $\mathbf{H}_{SD}\overline{\mathbf{v}} = \lambda_{\max} \mathbf{H}_{SX} \overline{\mathbf{v}}$, i.e., $\overline{\mathbf{v}}$ is the eigen vector corresponding to the largest eigen value λmax of the matrix $\mathbf{H}_{SX}^{\dagger} \mathbf{H}_{SD}$, where $\mathbf{H}_{SX}^{\dagger}$ indicates pseudo inverse of matrix $\mathbf{H}_{SX}$.

3. No-RIS Rule [9]: The SEP-optimal binary power control policy for no-RIS scenario, in the presence of direct S-D and direct S-X links, for the underlay spectrum sharing network subject to an average interference constraint is given in [9].

4. Random Phase Rule: The RIS phase shifts are randomly chosen from a uniform distribution between 0 and 2π.

To meet the average interference constraint, we adopt the following BPC policy for the EMSIR, no RIS, and random phase benchmarks. Let g denote the equivalent channel power gain from S to X using the corresponding phase shift choice as defined by the rule. If $P_{\max}\mathbb{E}[g] \leq I_{\text{th}}$, then we set $P_S = P_{\max}$. Else, let $\beta > 0$ is the unique solution of $P_{\max} \int_0^{\beta} x f_g(x)\, dx = I_{\text{th}}$, which is computed numerically. Then, we set $P_S = P_{\max}$, if $g \leq \beta$; otherwise, $P_S = 0$.

We see that all the rules employing binary power control satisfy the average interference constraint. (i) When $I_{\text{th}}/\sigma^2 < I_{\text{un}}/\sigma^2 = 19$ dB: In this Region II, the optimal rule in (41) is active and the average interference power becomes equal to I_{th}. Therefore, as I_{th} increases, we see that the normalized average interference power increases and the average SEP decreases due to relaxed interference constraint. The proposed optimal rule performs better by an order of magnitude than the other rules. We see that the LI rule, random phase rule, and no

Authorized licensed use limited to: Indian Institute of Technology. Downloaded on November 03,2026 at 17:26:23 UTC from IEEE Xplore. Restrictions apply.

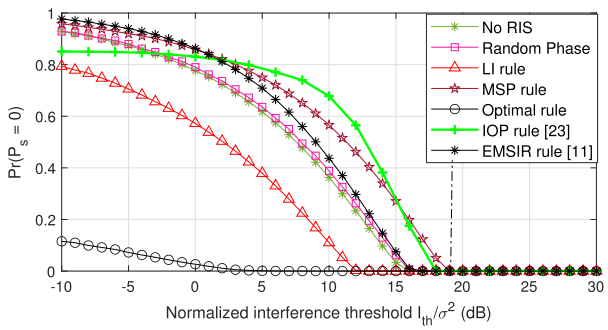
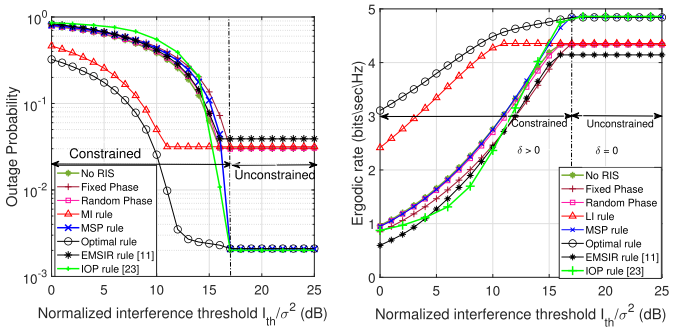


Fig. 9. Probability of $P_S = 0$ as a function of I_{th}/σ^2 ($M = 20$, $P_{\max} = 15$ dBm, $d_v = \lambda/4$, and 8PSK).



(a) Outage probability at D (b) Ergodic rate at D

Fig. 10. Outage probability and ergodic rate of the secondary network as a function of I_{th}/σ^2 ($\gamma_{\text{th}} = 0$ dB, $P_{\max} = 15$ dBm, $d_v = \lambda/4$, $M = 10$, and 8PSK).

RIS rule perform better than the MSP rule. This happens as the MSP rule selects zero transmit power option more often in order to meet the interference constraint, as shall be illustrated in Fig. 9. The SEP performance of the IOP and EMSIR rules are comparable with the MSP rule in this region. (ii) When $I_{\text{th}}/\sigma^2 \geq I_{\text{un}}/\sigma^2$: In this Region I, the unconstrained rule in (7) is optimal. Therefore, the normalized average interference power saturates at I_{un}/σ^2. The average SEP of the optimal rule floors to a value independent of I_{th}/σ^2, following the conventional non-spectrum sharing system without interference constraint. For this reason, the MSP rule provides the same average SEP as that of the optimal rule and both outperform the other rules. However, the IOP rule performs very close to the MSP and optimal rules in Region I due to the common objective of SEP minimization when interference constraint is relaxed. We also see that the average interference power at X by the optimal, MSP, and IOP rules match and saturates at I_{un}/σ^2. The EMSIR rule results the highest average SEP in this region. No RIS, EMSIR, and random phase rules cause lower interference than that of the optimal and MSP rules. We see that the average interference power of the LI rule is the lowest among all other rules due to the choice of RIS phase shifts to minimize the interference.

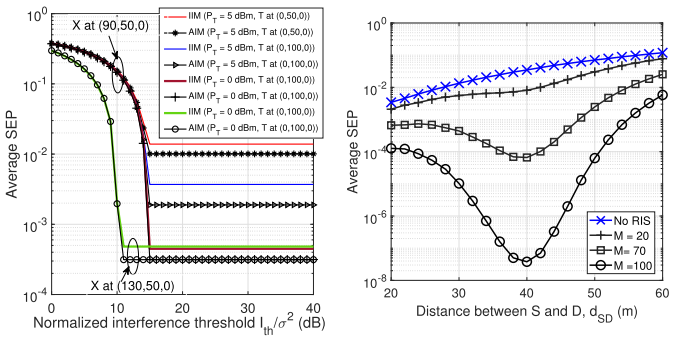
Probability of Zero Transmit Power: To understand the behaviour of the proposed rules, Fig. 9 plots the probability of zero transmit power ($P_S = 0$). It decreases as I_{th}/σ^2 increases. This is because the source transmits with zero power less often as the interference constraint is relaxed. We also see that $\Pr(P_S = 0)$ of the optimal rule is significantly lower than the other rules. For $I_{\text{th}}/\sigma^2 > 19$ dB, the interference constraint is inactive and all the rules trasnmit with $P_S = P_{\max}$. Hence, $\Pr(P_S = 0) = 0$.

Benchmarking for Outage Probability and Ergodic Rate: Fig. 10a plots the outage probability, i.e., the probability that the instantaneous SINR γ_S at D falls below a target threshold γ_{th}, as a function of normalized interference threshold I_{th}/σ^2. Fig. 10b plots the ergodic rate at D. Also shown is the fixed phase rule, in which the RIS phase shifts are kept fixed at 45°. For the optimal rule that is designed to minimize SEP, in the interference-constrained region, we see that as I_{th}/σ^2 increases, the outage probability decreases and the ergodic rate increases as the interference constraint is relaxed. However, in the interference-unconstrained region, they become independent of I_{th}/σ^2. We further note that, among all the rules, the proposed optimal rule has the lowest outage probability and highest ergodic rate. The LI rule performs better than the MSP, EMSIR, IOP, no RIS, random, and fixed phase rules in the interference-constrained region. However, its performance is worse in the interference-unconstrained region. As before, the no RIS rule and the random phase rule have similar performance. Moreover, the MSP rule matches the optimal rule in the interference-unconstrained region. The EMSIR rule incurs higher outage probability and lower ergodic rate in both the regions. The IOP rule provides similar outage probability and ergodic rate as that of the MSP and optimal rules in the interference-unconstrained region, while showcasing degraded performance in the interference-constrained region.

Effect of Primary Interference Model and Location of Various Nodes: Fig. 11a plots the average SEP of the secondary system of the optimal rule as a function of I_{th}/σ^2 for two different primary interference models with $M = 64$. This is done for different locations of primary receiver X, primary transmitter T and its transmit power P_T. We note that the SEP obtained by the average interference model (AIM) is slightly lower than that of the instantaneous interference model (IIM). We see that as the primary transmit power P_T decreases or T is located away from the secondary system, the average SEP at D decreases. This is due to the reduced interference power from T to the secondary system. When $P_T = 0$ dBm and T is at $[0, 100, 0]$, as X is moved further away from $[90, 50, 0]$ to $[130, 50, 0]$, we see that the average SEP decreases for lower I_{th}, since the probability that S transmits with peak power $P_{\max}$ increases. However, for higher I_{th}, the SEP values for both cases are the same, as S transmits with power $P_{\max}$ independent of the interference channel strength.

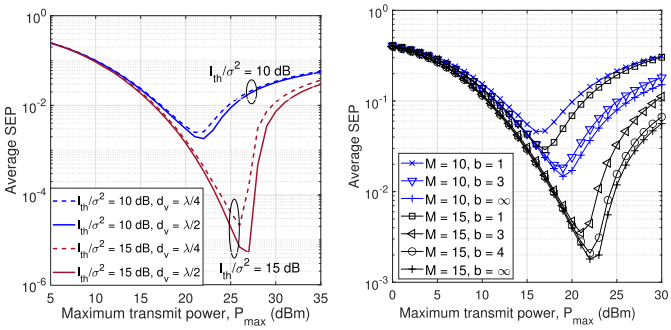
Fig. 11b plots the average SEP of the optimal rule as a function of S-D distance d_{SD} for different values of M. The locations of S, X, and the RIS are set as $[0, 0, 0]$, $[60, 0, 0]$, and $[40, 10, 0]$, respectively, and d_{SD} is varying. We also plot the average SEP for no RIS case [9]. Its average SEP increases as d_{SD} increases. However, using RIS with $M = 20$, we see that the average SEP initially increases as d_{SD} increases and then starts decreasing till $d_{SD} = 40$ m as D moves closer to the RIS and RIS-reflected link becomes stronger, though it moves away from S. Furthermore, the average SEP increases with d_{SD} for $d_{SD} > 40$ m. This is because D moves away from

Authorized licensed use limited to: Indian Institute of Technology. Downloaded on November 03,2026 at 17:26:23 UTC from IEEE Xplore. Restrictions apply.



(a) Primary interference models (b) Impact of RIS location

Fig. 11. (a) Impact of P_T, location of T and X considering both instantaneous and average interference model from T ($P_{\max} = 15$ dBm, 8PSK, $M = 64$, and $d_v = \lambda/4$, locations of S, D, and RIS as [0,0,0], [100,0,0], [98,0,10]), (b) Average SEP as a function of distance between S and D ($P_{\max} = 5$ dBm, $I_{\text{th}}/\sigma^2 = 20$ dB, $d_v = \lambda/4$, and 8PSK).



(a) Impact of I_{th} and d_v ($M = 20$) (b) Impact of M and b

Fig. 12. Average SEP as a function of $P_{\max}$ for 8PSK ($I_{\text{th}}/\sigma^2 = 15$ dB and $d_v = \lambda/4$ for (b)).

both S and the RIS. We further see that as M increases, the average SEP decreases, and the maximum benefit is observed when D is close to RIS ($d_{SD} = 40$ m). Thus, the placement of the RIS plays a crucial role.

Effect of $P_{\max}$, I_{th}, M, Spatial Correlation, and Discrete Phase Shifts: Fig. 12a plots the average SEP of the optimal rule as a function of $P_{\max}$. We see that as $P_{\max}$ increases, the average SEP decreases first. Thereafter, it increases and saturates at c_1 (c.f. (4)). This is because the optimal rule sets $P_S = 0$ more often for higher $P_{\max}$ to meet the average interference constraint. We note that as I_{th} increases, the SEP decreases due to relaxed interference constraint, and the transition point shift to the right. As the spacing between the reflecting elements d_v decreases, the average SEP increases due to increase in the spatial correlation.

Fig. 12b plots the average SEP of the optimal rule for different values of M considering the discrete phase shifts for the RIS. Let b denote the number of bits used to denote the 2^b discrete values that θ_m, $1 \le m \le M$ can take. For $b = 1$, the average SEP has increased than that of the continuous phase case ($b = \infty$). We note that the performance with $b = 3$ is very close to that of using continuous phase for $M = 10$. For $M = 15$, we observe that $b = 4$ is sufficient. Furthermore, as M increases, the average SEP decreases, showing the efficacy of using increased number of RIS elements.

Performance-Complexity Trade-off With Codebook Based Schemes [13], [14], [15], [41]: We consider a codebook $\mathcal{C}$ with K RIS reflection patterns to study the trade-off between computational time and the SEP performance of the proposed CSI-based scheme and codebook based schemes [41]. A reflection pattern that minimizes the same SEP–interference metric as the proposed optimal rule is selected as follows:

$$\left(\bar{P}_S, \bar{\boldsymbol{\Theta}}\right) = \underset{P_S, \boldsymbol{\Theta} \in \mathcal{C}}{\operatorname{argmin}} \left\{ \text{SEP}\left(P_S, \boldsymbol{\Theta}\right) + \delta I\left(P_S, \boldsymbol{\Theta}\right) \right\}, \quad (44)$$

where δ is obtained to satisfy the average interference constraint as earlier.

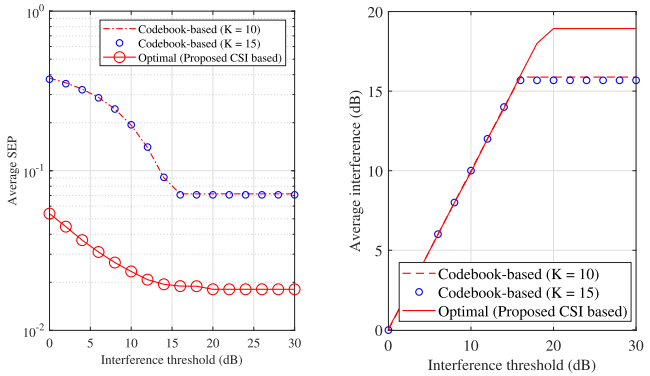
Fig. 13a and 13b plots the average SEP and average interference as a function of the interference threshold for the proposed instantaneous CSI based and codebook based scheme in (44). The average SEP of the CSI based scheme is approximately an order of magnitude lower than the codebook based scheme. However, both the schemes meet the interference constraint.

Computational Time: While the CSI-based schemes requires 14 s, the codebook-based scheme requires 4 s, on a computer with an Intel Core i7-12700 processor and 16 GB of RAM. Furthermore, we observed that for $M = 40$, the SEP of the codebook scheme degrades by a factor of $35\times$ at $I_{\text{th}}/\sigma^2 = 12$ dB while requiring $0.1\times$ computational time as that of the instantaneous CSI-based optimal scheme. The SEP performance loss is primarily due to suboptimal phase adaptation. Moreover, this gap becomes more pronounced with increasing RIS size.

SimRIS Channel Simulator for Practical Channel Modeling: We now demonstrate our result with practical channel simulator using the open-source *SimRIS Channel Simulator* following 3GPP standards [42]. These channels are widely used for link level and system level simulations for 6G. The locations of S, D, X, and the RIS are set as $[0, 25, 20]$, $[80, 75, 1]$, $[90, 55, 1]$, and $[70, 85, 10]$, respectively, and $M = 16$. Fig. 14(a) and (b) plot the average SEP at D and the normalized average interference power at X, respectively, for the MSP rule as a function of maximum transmit power $P_{\max}$. We see that as $P_{\max}$ increases, the average SEP decreases and the average interference power increases first. Thereafter, the average SEP increases since the MSP rule sets $P_S = 0$ more often for higher $P_{\max}$, to meet the average interference constraint. This is also prominent from the observation that the average interference power at X saturates at normalized interference threshold I_{th}/σ^2 for higher values of $P_{\max}$. We also note that as normalized interference threshold increases from 15 to 25 dB, the average SEP decreases, as we observed earlier in Fig 12(a). We note that the trends for the LI rule and optimal rule are the same, and we do not plot for brevity using the *SimRIS Channel Simulator*. This preliminarily computer simulation results reveal the practical use-cases of RIS in spectrum sharing scenario.

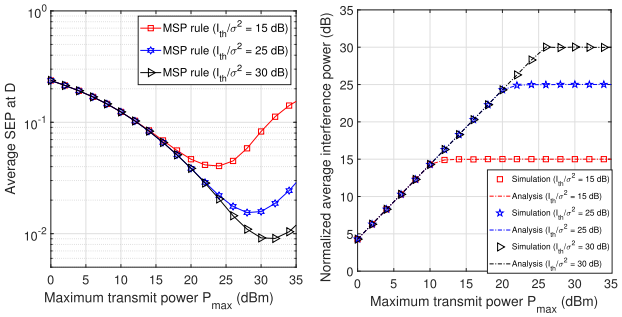
Effect of Imperfect CSI: Fig. (15)(a) and (b) plot the average SEP at D and the normalized average interference power at X, respectively, as a function of normalized interference threshold for $\sigma_I = \sigma_C = \sigma = 0.05$, where $1 - \sigma$ captures the channel estimation accuracy (c.f. (32)). We see that the average

Authorized licensed use limited to: Indian Institute of Technology. Downloaded on November 03,2026 at 17:26:23 UTC from IEEE Xplore. Restrictions apply.



(a) Average SEP (b) Average interference power

Fig. 13. Performance comparison of the proposed CSI based and the codebook based schemes as a function of I_{th}/σ^2 ($M = 20$, $P_{\max} = 15$ dBm, and 8PSK).

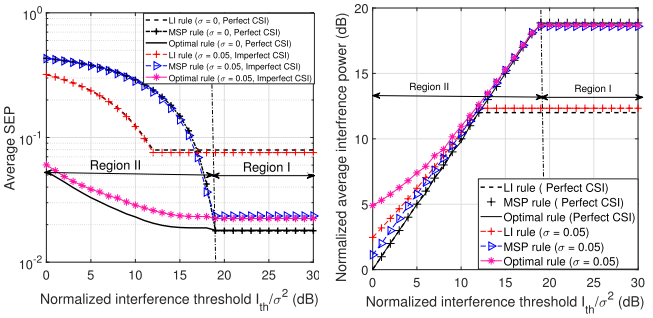


(a) Average SEP (b) Average interference power

Fig. 14. Average SEP at D and average interference power at X as a function of $P_{\max}$ of the MSP rule using *SimRIS Channel Simulator* ($M = 16$, $f_c = 28$ GHz, and QPSK).

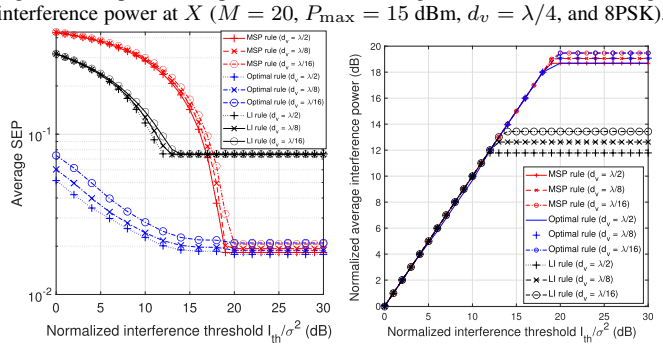
interference power by the MSP rule increases due to imperfect CSI than that of the perfect CSI case in Region-II, while the average SEP increases slightly than that of the perfect CSI case ($\sigma = 0$). However in the Region-I, the average SEP increases and the average interference power slightly reduces than that of the perfect CSI. This is because the MSP rule sets $\theta_m = \angle\hat{h}_{SD} - \angle\hat{C}_D(m)$, for $1 \le m \le M$, as a function of phase of the S-D and S-RIS-D channel gains estimates. For the optimal rule, the RIS phase shifts and power allocation of S depend on estimated values of S-D and S-X equivalent channel gains. Thus, it is more sensitive than that of the LI and MSP rules in Region II under imperfect CSI. We see that the LI rule, which sets the RIS phase shifts based on estimated channel gains of S-X links and S-RIS-X links, is less sensitive to channel estimation errors in terms of SEP performance. However, it results slightly increased average interference power than that of the MSP rule in Region II, while generating lower interference power among all three rules under imperfect CSI in Region I.

Effect of Sinc-based Correlation Model (1): Figs. 16 (a) and (b), respectively, plot the average SEP at D and the normalized average interference power at X of the optimal, MSP, and LI rules as a function of normalized interference threshold I_{th}/σ^2. Three varying RIS element spacing (d_v) is considered to capture the spatial correlation, as given in (1). For the MSP rule, as d_v decreases from $\lambda/2$ to $\lambda/8$ and $\lambda/16$,



(a) Average SEP (b) Average interference power

Fig. 15. Impact of imperfect CSI on average SEP at D and average interference power at X ($M = 20$, $P_{\max} = 15$ dBm, $d_v = \lambda/4$, and 8PSK).



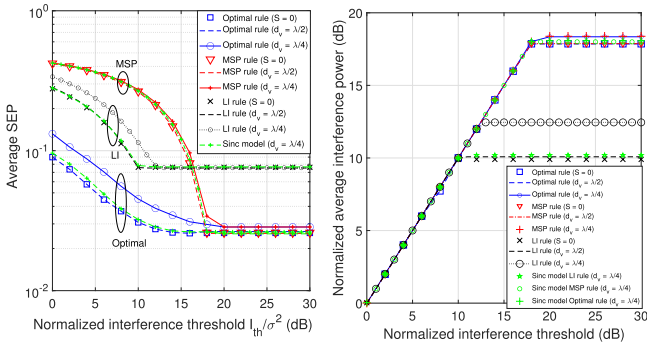
(a) Average SEP (b) Average interference power

Fig. 16. Impact of sinc-based correlation model on average SEP at D and average interference power at X as a function of I_{th}/σ^2 of the LI, MSP, and optimal rules ($M = 20$, $P_{\max} = 15$ dBm, $f = 10$ GHz, $\sigma^2 = -100$ dBm; and 8PSK).

we see that the average SEP increases for the entire range of I_{th} considered. This is due to increased spatial correlation with reduced RIS element spacing. We further see that the LI rule is less sensitive than the MSP rule w.r.t. relative SEP increment as d_v is decreasing. From Figure 16(b) we see that the average interference constraint is met even under spatial correlation. For low-to-mid values of I_{th} (interference-constrained regime), we see that as I_{th} increases, the average interference power becomes equal to I_{th} for all values of d_v. However, in the interference-unconstrained regime (for higher I_{th}), the normalized average interference power saturates at $I_{\text{avg}}^{\text{low}}/\sigma^2$. Moreover, its value slightly increases as d_v decreases (within interference threshold limit even for $d_v = \lambda/16$). The optimal rule provides the lowest SEP among all three rules. As d_v decreases, the average SEP increases and the average interference power floor at higher I_{th} increases by it. We notice that the MSP rule and the optimal rule perform the same in the interference-unconstrained region (for higher I_{th} values) in terms of average SEP and average interference power, which is as expected. Similar trend w.r.t. RIS element spacing can be observed as we increase no. of RIS reflecting elements M. We do not plot this for brevity.

Impact of Scattering Matrix-based Correlation Model (40): Figs. 17 (a) and (b) plot the average SEP at D and the normalized average interference power at X of the MSP, LI, and optimal rules as a function of normalized interference threshold I_{th}/σ^2. The scattering matrix-based correlation model with varying minimum RIS inter-element spacing d_v is used here. We note that similar trend is observed as that

Authorized licensed use limited to: Indian Institute of Technology. Downloaded on November 03,2026 at 17:26:23 UTC from IEEE Xplore. Restrictions apply.



(a) Average SEP (b) Average interference power

Fig. 17. Impact of scattering matrix-based correlation model on average SEP at D and average interference power at X as a function of I_{th}/σ^2 of the LI, and MSP rules ($M = 16$, $P_{\max} = 15$ dBm, $f = 10$ GHz, and 8PSK).

of sinc-based correlation model. The average SEP increases slightly by the scattering matrix-based correlation model and as d_v decreases to $\lambda/4$, its average interference power saturates at a higher value. Nevertheless, the average interference constraint is satisfied for all three schemes. We also show results obtained by the diagonal phase shift model ($\mathbf{S} = 0$) as a baseline reference, which provides the lowest average SEP. For comparison we also plot the sinc-based correlation model for all three rules using $d_v = \lambda/4$. It serves as a tight lower bound of the average SEP obtained by using the scattering matrix-based correlation model under same $d_v = \lambda/4$.

VII. Conclusion

For an RIS-assisted spectrum sharing system, we developed a novel SEP-optimal rule for joint binary power control and RIS passive beamforming subject to an average interference constraint that is practical yet less-investigated in literature. Our proof technique showed that the optimal rule minimizes the metric that is a linear combination of the instantaneous SEP and the instantaneous interference power scaled by an interference penalty factor δ, which required solving simultaneous equations numerically. We also proposed an algorithm to accurately compute optimal δ. To reduce complexity, we next proposed the LI rule and MSP rule, which compute the RIS phase shifts using closed-form expressions. We showed that binary power control policy for the two rules depend on a threshold of the effective channel power from S to X and it is chosen to meet the average interference constraint. We analytically obtained this threshold using the derived PDF of the effective channel power gain from S to X, which followed Gamma distribution. Considering spatial correlation of the RIS channels, we derived expressions for the average interference power at X for both the LI and MSP rules. We further derived their closed form asymptotic expressions for large M and obtained valuable insights.

Extensive benchmarking results showed that the optimal rule achieved the lowest average SEP than the other rules by an order of magnitude. Furthermore, it provided the lowest outage probability and the highest ergodic rate than the other rules. With binary power control and in the interference-constrained regime, we showed that the LI rule, which configured the RIS phase shifts to reduce interference power at X, had lower SEP and outage probability, and higher ergodic rate than the MSP rule, which configured the RIS phase shifts to maximize the received signal power at D. However, in the interference-unconstrained regime, the MSP rule performed significantly better than the LI rule. We further investigated the impact of imperfect CSI, RIS mutual coupling effect, and compared the instantaneous CSI-based scheme with the codebook-based scheme for RIS phase control, and gain performance versus complexity trade-offs. Our results showed that the choice of binary power control and RIS phase shifts plays a crucial role in improving the performance of the secondary system while controlling the interference power at the primary receiver. They would be useful to design practical RIS-assisted spectrum-sharing networks as validated by *SimRIS Channel Simulator* following 3GPP standards. Including continuous power control and multi-antenna technique to better utilize the available CSI and introduce spatial diversity benefits can be potential future research.

Appendix

A. Proof of Result 1

A selection rule that always chooses the zero transmit power option causes zero interference to X. It is, therefore, feasible for any I_{th}. Therefore, the set of all feasible selection rules is a non-empty set. Let ϕ be a feasible rule, for which $\mathbf{\Theta}$ be the RIS phase shift vector and P_S be the transmit power of S. For $\delta > 0$, define an auxiliary function $\mathcal{L}_\phi(\delta)$ associated with ϕ as follows:

$$\mathcal{L}_\phi(\delta) \triangleq \mathbb{E}\left[\text{SEP}\left(P_S, \mathbf{\Theta}\right) + \delta I\left(P_S, \mathbf{\Theta}\right)\right]. \tag{45}$$

Note that $\mathcal{L}_\phi(\delta)$ is a function of both ϕ and δ. Furthermore, we define $\overline{\phi}$ to be another feasible rule, which selects $\bar{P}_S$ and $\bar{\mathbf{\Theta}}$ as follows:

$$\left(\bar{P}_S, \bar{\mathbf{\Theta}}\right) = \underset{P_S, \mathbf{\Theta}}{\text{argmin}} \left\{\text{SEP}\left(P_S, \mathbf{\Theta}\right) + \delta I\left(P_S, \mathbf{\Theta}\right)\right\}, \tag{46}$$

where δ is chosen such that $\mathbb{E}\left[I\left(\bar{P}_S, \bar{\mathbf{\Theta}}\right)\right] = I_{\text{th}}$. It can be proved using the intermediate value theorem that such a unique choice of δ exists. The theorem can be applied on the basis of the following two facts: (i) $0 \leq I_{\text{th}} < I_{\text{un}}$ and (ii) It can be shown that the average interference is a continuous and monotonically decreasing function of δ for $\delta \geq 0$. Thus, $\overline{\phi}$ is a feasible rule. We now prove that $\overline{\phi}$ is the optimal rule.

From the definition of $\overline{\phi}$ in (46) it follows that $\mathcal{L}_{\overline{\phi}}(\delta) \leq \mathcal{L}_\phi(\delta)$. Therefore, using (45) we can write

$$\begin{aligned}&\mathbb{E}\left[\text{SEP}\left(\bar{P}_S, \bar{\mathbf{\Theta}}\right) + \delta I\left(\bar{P}_S, \bar{\mathbf{\Theta}}\right)\right] \\ &\leq \mathbb{E}\left[\text{SEP}\left(P_S, \mathbf{\Theta}\right) + \delta I\left(P_S, \mathbf{\Theta}\right)\right].\end{aligned} \tag{47}$$

Since $\mathbb{E}\left[I\left(\bar{P}_S, \bar{\mathbf{\Theta}}\right)\right] = I_{\text{th}}$, we get

$$\mathbb{E}\left[\text{SEP}\left(\bar{P}_S, \bar{\mathbf{\Theta}}\right)\right] \leq \mathbb{E}\left[\text{SEP}\left(P_S, \mathbf{\Theta}\right)\right] + \delta\left(\mathbb{E}\left[I\left(P_S, \mathbf{\Theta}\right)\right] - I_{\text{th}}\right). \tag{48}$$

Since ϕ is a feasible rule, we know that $\mathbb{E}\left[I\left(P_S, \mathbf{\Theta}\right)\right] - I_{\text{th}} \leq 0$. Moreover, as $\delta > 0$, this ensures that

$$\mathbb{E}\left[\text{SEP}\left(\bar{P}_S, \bar{\mathbf{\Theta}}\right)\right] \leq \mathbb{E}\left[\text{SEP}\left(P_S, \mathbf{\Theta}\right)\right]. \tag{49}$$

Hence, $\overline{\phi}$ in (46) yields the lowest average SEP among all feasible rules and is indeed the optimal rule.

Authorized licensed use limited to: Indian Institute of Technology. Downloaded on November 03,2026 at 17:26:23 UTC from IEEE Xplore. Restrictions apply.

B. Proof of Result 2

Averaging (14) over channel fades, we get,

$$I_{\text{avg}}^{\text{low}} = \mathbb{E}[I(P_S, \boldsymbol{\Theta})] = A_1 + A_2 - A_3, \tag{50}$$

where

$$A_1 = P_{\max}\mathbb{E}\left[|h_{SX}|^2\right] = P_{\max}\mu_{SX}, \tag{51}$$

$$A_2 = P_{\max}\mathbb{E}\left[\left(\sum_{m=1}^{M}|h_{RX}^m|\,|h_{SR}^m|\right)^2\right], \tag{52}$$

$$A_3 = 2P_{\max}\mathbb{E}\left[|h_{SX}|\sum_{m=1}^{M}|h_{RX}^m|\,|h_{SR}^m|\right]. \tag{53}$$

We now simplify A_2 and A_3 separately.

Evaluating A_2: Now, $A_2 = P_{\max}\mathbb{E}\left[\sum_{m=1}^{M}|h_{RX}^m|^2|h_{SR}^m|^2 + \sum_{m=1}^{M}\sum_{n=1n\neq m}^{M}|h_{RX}^m|\,|h_{SR}^m|\,|h_{RX}^n|\,|h_{SR}^n|\right]$. Since the RVs, h_{RX}^m and h_{SR}^m are independent and $\mathbb{E}[|h_{RX}^m|^2] = \mu_{RX}$, $\mathbb{E}[|h_{SR}^m|^2] = \mu_{SR}$, the above expression can be simplified as $A_2 = P_{\max}M\mu_{RX}\mu_{SR} + P_{\max}\sum_{m=1}^{M}\sum_{n=1n\neq m}^{M}\mathbb{E}\left[|h_{RX}^m|\,|h_{RX}^n|\right]\mathbb{E}\left[|h_{SR}^m|\,|h_{SR}^n|\right]$. We note that $|h_{\mathcal{XY}}^m|$ and $|h_{\mathcal{XY}}^n|$ are two correlated Rician RVs. Using [43, (7)], $\mathbb{E}\left[|h_{\mathcal{XY}}^m||h_{\mathcal{XY}}^n|\right]$ can be expressed as (19).

Evaluating A_3: Since the direct S-X link channel gain h_{SX} is independent of S-RIS channel gain h_{SR}^m and RIS-X link channel gain h_{RX}^m, the term A_3 in (53) simplifies to $A_3 = 2P_{\max}\mathbb{E}[|h_{SX}|]\sum_{m=1}^{M}\mathbb{E}[|h_{RX}^m|]\,\mathbb{E}[|h_{SR}^m|]$. Since h_{SR}^m and h_{RX}^m undergo Rician fading, $\mathbb{E}[|h_{SR}^m|] = \sqrt{\frac{\pi\mu_{SR}}{4(K_{SR}+1)}}L_{1/2}\left(-K_{SR}\right)$ and $\mathbb{E}[|h_{RX}^m|] = \sqrt{\frac{\pi\mu_{RX}}{4(K_{RX}+1)}}L_{1/2}\left(-K_{RX}\right)$. Since h_{SX} undergoes Rayleigh fading, $\mathbb{E}[|h_{SX}|] = \sqrt{\pi\mu_{SX}}/2$. Substituting these in above A_3, yields the closed form expression in (17).

C. Proof of Result 3

When $\theta_m = \pi + \theta_{h_{SX}} - \left(\theta_{h_{SR}^m} + \theta_{h_{RX}^m}\right)$, for $1 \leq m \leq M$, and $P_S = P_{\max}$, the instantaneous interference power at X normalized by M^2 is given by $P_{\max}\left(\frac{|h_{SX}|}{M} - \frac{\sum_{m=1}^{M}|h_{RX}^m||h_{SR}^m|}{M}\right)^2$. For large M, substituting (21) in this and averaging yields

$$\lim_{M\to\infty}\frac{I_{\text{avg}}^{\text{low}}}{M^2} \to P_{\max}\mathbb{E}\left[\left(\frac{|h_{SX}|}{M} - \tau\sqrt{\mu_{SR}\mu_{RX}}\right)^2\right], \tag{54}$$

where τ is given in (20). Upon further simplification using $\mathbb{E}\left[|h_{SX}|^2\right] = \mu_{SX}$ and $\mathbb{E}\left[|h_{SX}|\right] = \sqrt{\pi\mu_{SX}}/2$, we get the desired result in (22).

D. Proof of Result 4

We simplify here the term T_5. Three expectation terms in (26) can be derived as follows:

(i) $\mathbb{E}\left[h_{RX}^m\left(h_{RX}^n\right)^*\right]$: Let $X_1 \triangleq h_{RX}^m$ and $X_2 \triangleq h_{RX}^n$. Define $\mathbf{V} = [X_1, X_1]^T \sim \mathcal{CN}(\mathbf{m}, \Sigma)$ be a two dimensional complex Gaussian random vector with the mean vector $\mathbf{m}$ and covariance matrix Σ are given by

$$\mathbf{m} = \mathbb{E}[\mathbf{V}] = [m_{X_1}, m_{X_2}]^T, \tag{55}$$

$$\Sigma = \mathbb{E}\left[(\mathbf{V}-\mathbf{m})(\mathbf{V}-\mathbf{m})^H\right] = \begin{bmatrix}\sigma_{X_1}^2 & \rho_{m,n}\sigma_{X_1}\sigma_{X_2}\\ \rho_{m,n}\sigma_{X_1}\sigma_{X_2} & \sigma_{X_2}^2\end{bmatrix}, \tag{56}$$

where $m_{X_1} = m_{X_2} = \sqrt{\mu_{RX}K_{RX}/(1+K_{RX})}$, $\sigma_{X_1}^2 = \sigma_{X_2}^2 = \mu_{RX}/(1+K_{RX})$, and $\rho_{m,n} = [\mathbf{C}]_{m,n}$. Therefore, $\mathbb{E}\left[h_{RX}^m\left(h_{RX}^n\right)^*\right]$ in (26) reduces to

$$\rho_{m,n}\sigma_{X_1}\sigma_{X_2} + m_{X_1}m_{X_2}^* = \frac{(\rho_{m,n}+K_{RX})\mu_{RX}}{1+K_{RX}}. \tag{57}$$

(ii) $\mathbb{E}[|h_{SR}^m||h_{SR}^n|]$: This can obtained by using $\mathcal{XY} \in \{SR\}$ in (19).

(iii) $\mathbb{E}\left[\exp\left(j\left(\theta_{h_{RD}^n} - \theta_{h_{RD}^m}\right)\right)\right]$: Let $Y_1 \triangleq h_{RD}^m$, $Y_2 \triangleq h_{RD}^n$, and $Z = Y_1^*Y_2$. Expressing Z in polar coordinates, we get $Z = Re^{j\Theta}$, where $R = |h_{RD}^m|\,|h_{RD}^n|$ and $\Theta = \left(\theta_{h_{RD}^n} - \theta_{h_{RD}^m}\right)$. The joint pdf of (R,Θ) can be shown to be [44, (5)]:

$$f_{R,\Theta}(r,\theta) = \frac{2re^{-g(r,\theta)}}{c\pi\sigma_y^2}\sum_{q=0}^{\infty}\sum_{p=0}^{\infty}\frac{(\beta_1(r))^q\,\beta_2^p}{q!p!\left(\beta_3(r,\theta)\right)^{\frac{q+p}{2}}} \times\left(\frac{r^2}{c\alpha}\right)^{\frac{p-q}{2}}K_{p-q}\left(2r\sqrt{\frac{\alpha}{c}}\right)I_{p+q}\left(2\sqrt{\beta_3(r,\theta)}\right), \tag{58}$$

where $m_{Y_1} = m_{Y_2} = \sqrt{\mu_{RD}K_{RD}/(1+K_{RD})}$, $\sigma_{Y_1}^2 = \sigma_{Y_2}^2 = \mu_{RD}/(1+K_{RD})$, $\alpha = \frac{|b|^2}{c} + \frac{1}{\sigma_{Y_1}^2}$, $g(r,\theta) = \frac{|a|^2 - 2\Re\{rbe^{-j\theta}\}}{c} + \frac{|m_{Y_1}^2|}{\sigma_{Y_1}^2}$, $\beta_1(r) = \frac{r^2|a|^2}{c^2}$, $\beta_2 = \left|\frac{-b^*a}{c} + \frac{m_{Y_1}}{\sigma_{Y_1}^2}\right|^2$, $\beta_3(r,\theta) = 2\Re\left\{\frac{re^{-j\theta}a}{c}\left(\frac{-ba*}{c} + \frac{m_{Y_1}^*}{\sigma_{Y_1}^2}\right)\right\}$, in which $a = m_{Y_2} - \frac{\rho_{m,n}\sigma_{Y_2}}{\sigma_{Y_1}}m_{Y_1}$, $b = \frac{\rho_{m,n}\sigma_{Y_2}}{\sigma_{Y_1}}$, $c = \sigma_{Y_2}^2\left(1-|\rho_{m,n}|^2\right)$, $I_n(z)$ is the modified Bessel function of the first kind with order n [35, (9.6.19)], and $K_n(z)$ denotes the modified Bessel function of the second kind with order n [35, (9.6.22)]. For large $|z|$, we can approximate $K_n(z)$ as $K_n(z) \approx \sqrt{\pi/(2z)}e^{-z}$ [35, (9.7.2)].

Moreover, the doubly-infinite summation in (58) can be evaluated by using finite number of terms in the upper limit. It is validated in [44] that the truncation error is faster than the exponential. Hence, we can use the upper limit as $\kappa = 10$.

The marginal PDF of Θ is given by $f_\Theta(\theta) = \int_0^\infty f_{R,\Theta}(r,\theta)\,dr$. Using (58), it can be expressed as

$$f_\Theta(\theta) \approx \sum_{q=0}^{\kappa}\sum_{p=0}^{\kappa}\int_{r=0}^{\infty}\frac{2re^{-g(r,\theta)}\left(\beta_1(r)\right)^q\beta_2^p}{c\pi\sigma_Y^2 q!p!\left(\beta_3(r,\theta)\right)^{\frac{q+p}{2}}}\left(\frac{r^2}{c\alpha}\right)^{\frac{p-q}{2}} \times I_{p+q}\left(2\sqrt{\beta_3(r,\theta)}\right)\sqrt{\frac{\pi}{4r\sqrt{\frac{\alpha}{c}}}}e^{-2r\sqrt{\frac{\alpha}{c}}}\,dr. \tag{59}$$

Substituting $2r\sqrt{\alpha/c} = x$, (59) can be simplified as

$$f_\Theta(\theta) \approx \sum_{q=0}^{\kappa}\sum_{p=0}^{\kappa}\int_{x=0}^{\infty}e^{-x}\chi_{q,p}^{RD}(x,\theta)\,dx, \tag{60}$$

where

$$\chi_{q,p}^{RD}(x,\theta) = xe^{-g\left(\frac{x}{2\sqrt{\frac{\alpha}{c}}},\theta\right)}\sqrt{\frac{\pi}{2x}}\left(\beta_1\left(\frac{x}{\sqrt{2\frac{\alpha}{c}}}\right)\right)^q(\beta_2)^p$$

Authorized licensed use limited to: Indian Institute of Technology. Downloaded on November 03,2026 at 17:26:23 UTC from IEEE Xplore. Restrictions apply.

$$\times \frac{\left(\frac{x}{2\alpha}\right)^{p-q} I_{q+p}\left(2\sqrt{\beta_3\left(\frac{x}{2\sqrt{\frac{\alpha}{c}}},\theta\right)}\right)}{2\pi\alpha\sigma_Y^2 q!p!\left(\beta_3\left(\frac{x}{2\sqrt{\frac{\alpha}{c}}},\theta\right)\right)^{\frac{p+q}{2}}}. \quad (61)$$

Low Complexity Implementation: By using Gauss-Laguerre quadrature [35, (25.4.45)], the above integral in (60) can be approximated as

$$f_\Theta(\theta) \approx \sum_{q=0}^{\kappa}\sum_{p=0}^{\kappa}\sum_{i=1}^{N} w_i \chi_{q,p}^{RD}(x_i,\theta), \quad (62)$$

where x_i and w_i, for $1 \le i \le N$, are N Gauss Laguerre abscissas and weights, respectively. We have found that just $N = 5$ terms are sufficient for the system parameters of interest. The mean value of $e^{j\Theta}$ is given by $\mathbb{E}\left[e^{j\Theta}\right] = \int_{-\pi}^{\pi} e^{j\theta} f_\Theta(\theta)\, d\theta$. As $\Theta = \left(\theta_{h_{RD}^n} - \theta_{h_{RD}^m}\right)$, we get from (62)

$$\mathbb{E}\left[e^{j\left(\theta_{h_{RD}^n} - \theta_{h_{RD}^m}\right)}\right] \approx \sum_{q=0}^{\kappa}\sum_{p=0}^{\kappa}\sum_{i=1}^{N} w_i \int_{-\pi}^{\pi} e^{j\theta}\chi_{q,p}^{RD}(x_i,\theta)\, d\theta. \quad (63)$$

Combining all the necessary terms yields (27).

REFERENCES

[1] P. Das, S. Kashyap, R. Sarvendranath, and A. Mishra, "Binary power control and passive beamforming for RIS-assisted spectrum sharing network," in *Proc. IEEE Globecom Workshops (GC Wkshps)*, Dec. 2023, pp. 1621–1626.

[2] J. Yuan, Y.-C. Liang, J. Joung, G. Feng, and E. G. Larsson, "Intelligent reflecting surface-assisted cognitive radio system," *IEEE Trans. Commun.*, vol. 69, no. 1, pp. 675–687, Jan. 2021.

[3] M. Matinmikko-Blue, S. Yrjölä, and P. Ahokangas, "Spectrum management in the 6G era: The role of regulation and spectrum sharing," in *Proc. 2nd 6G Wireless Summit (6G SUMMIT)*, Mar. 2020, pp. 1–5.

[4] *World Radiocommunication Conference 2023: Provisional Final Acts, ITU-R*, Geneva, Switzerland, Nov. 2023.

[5] *Amendment of the Commission's Rules With Regard to Commercial Operations in the 3550–3650 MHz Band, FCC*, Washington, DC, USA, Feb. 2015.

[6] C. Tarver et al., "Enabling a 'use-or-share' framework for PAL-GAA sharing in CBRS networks via reinforcement learning," *IEEE Trans. Cognit. Commun. Netw.*, vol. 5, no. 3, pp. 716–729, Sep. 2019.

[7] B. Chen, J. Chen, Y. Gao, and J. Zhang, "Coexistence of LTE-LAA and Wi-Fi on 5 GHz with corresponding deployment scenarios: A survey," *IEEE Commun. Surveys Tuts.*, vol. 19, no. 1, pp. 7–32, 1st Quart., 2017.

[8] R. Liebhart, M. Shafi, H. Tataria, G. Shivanandan, and D. Chandramouli, "Perspectives on 6G architectures," *IEEE Wireless Commun.*, vol. 32, no. 1, pp. 108–114, Feb. 2025.

[9] S. Kashyap and N. B. Mehta, "Optimal binary power control for underlay CR with different interference constraints and impact of channel estimation errors," *IEEE Trans. Commun.*, vol. 62, no. 11, pp. 3753–3764, Nov. 2014.

[10] R. Sarvendranath and N. B. Mehta, "Transmit antenna selection for interference-outage constrained underlay CR," *IEEE Trans. Commun.*, vol. 66, no. 9, pp. 3772–3783, Sep. 2018.

[11] X. Guan, Q. Wu, and R. Zhang, "Joint power control and passive beamforming in IRS-assisted spectrum sharing," *IEEE Commun. Lett.*, vol. 24, no. 7, pp. 1553–1557, Jul. 2020.

[12] D. Xu, X. Yu, and R. Schober, "Resource allocation for intelligent reflecting surface-assisted cognitive radio networks," in *Proc. IEEE 21st Int. Workshop Signal Process. Adv. Wireless Commun. (SPAWC)*, May 2020, pp. 1–5.

[13] X. Jia, J. An, H. Liu, H. Liao, L. Gan, and C. Yuen, "Environment-aware codebook for reconfigurable intelligent surface-aided MISO communications," *IEEE Wireless Commun. Lett.*, vol. 12, no. 7, pp. 1174–1178, Jul. 2023.

[14] X. Jia, J. An, L. Gan, and H. Li, "Low-overhead dynamic codebook design for RIS-aided multiuser MISO systems," *Signal Process.*, vol. 244, Jul. 2026, Art. no. 110551.

[15] A. Papadopoulos et al., "On modeling the RIS as a resource: Multi-user allocation and efficiency-proportional pricing," *IEEE Trans. Netw. Service Manage.*, vol. 22, no. 5, pp. 4694–4705, Oct. 2025.

[16] L. Zhang, Y. Wang, W. Tao, Z. Jia, T. Song, and C. Pan, "Intelligent reflecting surface aided MIMO cognitive radio systems," *IEEE Trans. Veh. Technol.*, vol. 69, no. 10, pp. 11445–11457, Oct. 2020.

[17] V. Kumar, M. F. Flanagan, R. Zhang, and L.-N. Tran, "Achievable rate maximization for underlay spectrum sharing MIMO system with intelligent reflecting surface," *IEEE Wireless Commun. Lett.*, vol. 11, no. 8, pp. 1758–1762, Aug. 2022.

[18] X. Yuan, W. Li, Y. Hu, and A. Schmeink, "Beamforming design and resource allocation for IRS-assisted NOMA cognitive radio system," in *Proc. Int. Symp. Wireless Commun. Syst. (ISWCS)*, Oct. 2022, pp. 1–6.

[19] J. He, K. Yu, Y. Zhou, and Y. Shi, "Reconfigurable intelligent surface enhanced cognitive radio networks," in *Proc. IEEE 92nd Veh. Technol. Conf. (VTC-Fall)*, Nov. 2020, pp. 1–5.

[20] L. Zhang, C. Pan, Y. Wang, H. Ren, and K. Wang, "Robust beamforming design for intelligent reflecting surface aided cognitive radio systems with imperfect cascaded CSI," *IEEE Trans. Cognit. Commun. Netw.*, vol. 8, no. 1, pp. 186–201, Mar. 2022.

[21] I. Hameed, M. R. Camana, P. V. Tuan, and I. Koo, "Intelligent reflecting surfaces for sum-rate maximization in cognitive radio enabled wireless powered communication network," *IEEE Access*, vol. 11, pp. 16021–16031, 2023.

[22] Y. H. Al-Badarneh, M. K. Alshawaqfeh, O. S. Badarneh, and Y. M. Khattabi, "Performance analysis of RIS-assisted spectrum sharing systems," *IEEE Trans. Cognit. Commun. Netw.*, vol. 11, no. 1, pp. 465–474, Feb. 2025.

[23] P. Das, S. Ghosh, S. Kashyap, and R. Sarvendranath, "Role of interference-outage constraint and binary power control for RIS-assisted spectrum sharing," in *Proc. IEEE Wireless Commun. Netw. Conf. (WCNC)*, Mar. 2025, pp. 1–7.

[24] X. Guan and Q. Wu, "IRS-enabled spectrum sharing: Interference modeling, channel estimation and robust passive beamforming," *ZTE Commun.*, vol. 20, no. 1, pp. 28–35, Mar. 2022.

[25] R. Sarvendranath and N. B. Mehta, "Statistical CSI driven transmit antenna selection and power adaptation in underlay spectrum sharing systems," *IEEE Trans. Commun.*, vol. 69, no. 5, pp. 2923–2934, May 2021.

[26] R. Sarvendranath and N. B. Mehta, "Impact of multiple primaries and partial CSI on transmit antenna selection for interference-outage constrained underlay CR," *IEEE Trans. Wireless Commun.*, vol. 18, no. 2, pp. 942–953, Feb. 2019.

[27] P. Das and N. B. Mehta, "Rate-optimal relay selection for average interference-constrained underlay CR," *IEEE Trans. Commun.*, vol. 65, no. 12, pp. 5137–5148, Dec. 2017.

[28] P. Das, N. B. Mehta, and G. Singh, "Novel relay selection rules for average interference-constrained cognitive AF relay networks," *IEEE Trans. Wireless Commun.*, vol. 14, no. 8, pp. 4304–4315, Aug. 2015.

[29] E. Björnson and L. Sanguinetti, "Rayleigh fading modeling and channel hardening for reconfigurable intelligent surfaces," *IEEE Wireless Commun. Lett.*, vol. 10, no. 4, pp. 830–834, Apr. 2021.

[30] S. Taek Chung and A. J. Goldsmith, "Degrees of freedom in adaptive modulation: A unified view," *IEEE Trans. Commun.*, vol. 49, no. 9, pp. 1561–1571, Sep. 2001.

[31] J. Yuan, Y.-C. Liang, J. Joung, G. Feng, and E. G. Larsson, "Intelligent reflecting surface (IRS)-enhanced cognitive radio system," in *Proc. IEEE Int. Conf. Commun. (ICC)*, Jun. 2020, pp. 1–6.

[32] P. Appalla and P. Das, "Optimal relay and antenna selection in MIMO spectrum sharing relay networks under different CSI and interference constraints," *IEEE Open J. Commun. Soc.*, vol. 6, pp. 8965–9007, 2025.

[33] I. S. Gradshteyn and I. M. Ryzhik, *Table of Integrals, Series and Products*, 4th ed., New York, NY, USA: Academic, 1980.

[34] N. Costilla-Enriquez, Y. Weng, and B. Zhang, "Combining Newton–Raphson and stochastic gradient descent for power flow analysis," *IEEE Trans. Power Syst.*, vol. 36, no. 1, pp. 514–517, Jan. 2021.

[35] M. Abramowitz and I. Stegun, *Handbook of Mathematical Functions With Formulas, Graphs, and Mathematical Tables*, 9th ed., New York, NY, USA: Dover, 1972.

[36] R. Sarvendranath, A. K. R. Chavva, and E. G. Larsson, "Optimal antenna selection and beamforming for an IRS assisted system," *IEEE Trans. Wireless Commun.*, vol. 22, no. 9, pp. 5698–5710, Sep. 2023.

Authorized licensed use limited to: Indian Institute of Technology. Downloaded on November 03,2026 at 17:26:23 UTC from IEEE Xplore. Restrictions apply.

[37] Z. Luo, Y. Zhan, and E. Jonckheere, "Analysis on functions and characteristics of the Rician phase distribution," in *Proc. IEEE/CIC Int. Conf. Commun. China (ICCC)*, China, Aug. 2020, pp. 306–311.
[38] Q.-U.-A. Nadeem, H. Alwazani, A. Kammoun, A. Chaaban, M. Debbah, and M.-S. Alouini, "Intelligent reflecting surface-assisted multi-user MISO communication: Channel estimation and beamforming design," *IEEE Open J. Commun. Soc.*, vol. 1, pp. 661–680, 2020.
[39] D. Wijekoon, A. Mezghani, and E. Hossain, "Phase shifter optimization in RIS-aided MIMO systems under multiple reflections," *IEEE Trans. Wireless Commun.*, vol. 23, no. 8, pp. 8969–8983, Aug. 2024.
[40] P. Zheng, R. Wang, A. Shamim, and T. Y. Al-Naffouri, "Mutual coupling in RIS-aided communication: Model training and experimental validation," *IEEE Trans. Wireless Commun.*, vol. 23, no. 11, pp. 17174–17188, Nov. 2024.
[41] S. Ganesan, N. B. Mehta, and R. Sarvendranath, "Codebook-based IRS system: Impact of channel estimation errors and pilot power adaptation on codeword selection and data rate," *IEEE Trans. Wireless Commun.*, vol. 23, no. 12, pp. 19902–19915, Dec. 2024.
[42] E. Basar and I. Yildirim, "SimRIS channel simulator for reconfigurable intelligent surface-empowered communication systems," in *Proc. IEEE Latin-Amer. Conf. Commun. (LATINCOM)*, Nov. 2020, pp. 1–6.
[43] S. Dhok and P. K. Sharma, "Rate-splitting multiple access with STAR RIS over spatially-correlated channels," *IEEE Trans. Commun.*, vol. 70, no. 10, pp. 6410–6424, Oct. 2022.
[44] Y. Li, Q. He, and R. S. Blum, "On the product of two correlated complex Gaussian random variables," *IEEE Signal Process. Lett.*, vol. 27, pp. 16–20, 2020.



Priyanka Das (Senior Member, IEEE) received the Bachelor of Science degree (Hons.) in Physics from Burdwan Raj College, the University of Burdwan, West Bengal, India, in 2006, the Bachelor of Technology degree in radio physics and electronics from the University of Calcutta, West Bengal, India, in 2009, the Master of Technology degree in digital signal processing from Indian Institute of Technology (IIT) Guwahati, Guwahati, India, in 2011, and the Ph.D. degree from the Department of Electrical Communication Engineering, Indian Institute of Science, Bengaluru, India, in 2018. She was with Dell Research and Development, Bengaluru, from August 2011 to July 2012. In 2015, she was with Nokia Solutions Networks, Bengaluru, as a Summer Intern. She is currently an Assistant Professor with the Department of Electronics and Communication Engineering, International Institute of Information Technology Bangalore (IIIT-B), India. Her research interests include machine learning for wireless communication, multiple antenna techniques, spectrum sharing, reconfigurable intelligent surface, physical-layer security, and design and performance analysis for next-generation wireless networks.



Sumukha Kashyap (Student Member, IEEE) received the Bachelor of Technology degree in electronics and communications engineering from the R. V. College of Engineering, Bengaluru, India, in 2016, and the Master of Science (by Research) degree from the Department of Electronics and Communication Engineering, International Institute of Information Technology Bangalore (IIIT-B), India, in 2024. He is currently pursuing the Ph.D. degree with the Department of Electrical Engineering, IIT Madras, Chennai, India. From 2016 to 2021, he was a Contract Software Engineer with Cisco Systems Inc., Bengaluru, through Wipro Ltd. His current research interests include reconfigurable intelligent surfaces, sparse signal recovery, error control coding, deep learning, and their applications in wireless communication.



Rimalapudi Sarvendranath (Senior Member, IEEE) received the Bachelor of Technology degree in electrical and electronics engineering from the National Institute of Technology Karnataka, Surathkal, in 2009, and the Master of Engineering and Ph.D. degrees from the Department of Electrical Communication Engineering, Indian Institute of Science, Bengaluru, India, in 2012 and 2020, respectively. In 2021, he was a Post-Doctoral Researcher with the Department of Electrical Engineering, Linköping University, Sweden. He was an Assistant Professor with the Department of Electronics and Electrical Engineering, Indian Institute of Technology Guwahati, from January 2022 to June 2023. From 2012 to 2016, he was with Broadcom Communications Technologies, Bengaluru, where he worked on developing and implementing algorithms for LTE and IEEE 802.11ac wireless standards. He is currently an Assistant Professor with the Department of Electrical Engineering, Indian Institute of Technology Tirupati. His research interests include machine learning for wireless communication, multiple antenna techniques, spectrum sharing, and next-generation wireless standards.



Amrita Mishra (Member, IEEE) received the B.Tech. degree (Hons.) in electronics and communication engineering from the Amrita School of Engineering, Coimbatore, India, in 2011, and the joint M.Tech. and Ph.D. degrees from the Department of Electrical Engineering, IIT Kanpur, India, in 2018. She is currently the Infosys Foundation Career Development Chair Professor and an Assistant Professor with the Department of Electronics and Communication Engineering, International Institute of Information Technology Bangalore (IIIT-B), India. Her research interests include physical layer technologies for next-generation wireless communication systems, signal processing for communication applications, and machine learning techniques for 5G and beyond wireless networks. Her work spans the design and optimization of intelligent and high-performance communication systems for future wireless standards.

Authorized licensed use limited to: Indian Institute of Technology. Downloaded on November 03,2026 at 17:26:23 UTC from IEEE Xplore. Restrictions apply.